Cyclic Operation of a Semi-Batch Reactor for the Hydroformylation of Long-Chain Olefins and Integration in a Continuous Production Process

Karsten H.G. Rätze, Michael Jokiel, Nicolas M. Kaiser, Kai Sundmacher

PII: S1385-8947(18)32385-4
DOI: https://doi.org/10.1016/j.cej.2018.11.151
Reference: CEJ 20453

To appear in: *Chemical Engineering Journal*

Received Date: 12 June 2018
Revised Date: 16 November 2018
Accepted Date: 19 November 2018

Please cite this article as: K.H.G. Rätze, M. Jokiel, N.M. Kaiser, K. Sundmacher, Cyclic Operation of a Semi-Batch Reactor for the Hydroformylation of Long-Chain Olefins and Integration in a Continuous Production Process, *Chemical Engineering Journal* (2018), doi: https://doi.org/10.1016/j.cej.2018.11.151

Cyclic Operation of a Semi-Batch Reactor for the Hydroformylation of Long-Chain Olefins and Integration in a Continuous Production Process

Karsten H. G. Rätze[a], Michael Jokiel[b], Nicolas M. Kaiser[a], and Kai Sundmacher[a,b,*]

[a] *Otto von Guericke University Magdeburg, Chair for Process Systems Engineering, Universitätsplatz 2, D-39106 Magdeburg, Germany*

[b] *Max Planck Institute for Dynamics of Complex Technical Systems, Department Process Systems Engineering, Sandtorstr. 1, D-39106 Magdeburg, Germany*

[*] *sundmacher@mpi-magdeburg.mpg.de*

Abstract

The transition to renewable feedstocks in chemicals production requires innovative processes which are able to exploit the special properties of the feed material while still maintaining high process performance. Flexible semi-batch processes offer the advantage of dynamic adaptation to changing process requirements but suffer in terms of automation and production capacity where continuous processes excel. Combining the flexibility of a semi-batch reactor with the reliability of a continuous downstream process is the motivation for the application of a repeatedly operated semi-batch

reactor (RSBR) concept to the hydroformylation of 1-dodecene in a n-decane/DMF thermomorphic multiphase system (TMS). In order to predict the dynamic process behavior, a detailed dynamic process model is introduced and compared to a corresponding steady-state model. In addition, the RSBR concept is embedded in a miniplant process to prove its feasibility and convergence to a cyclic steady-state experimentally. Finally, the collected experimental data is compared to the results from the dynamic process model indicating accurate predictions of the integral process behavior.

Keywords: Hydroformylation; homogeneous catalysis; long-chain olefin; repeated semi-batch; dynamic simulation

1. Introduction

The production of chemicals can generally be divided into two major categories: commodity (bulk) and fine (specialty) chemical production. They are differentiated due to varying requirements with respect to process capacity, flexibility, product quality as well as applicability of automation. The product demand for fine chemicals is normally moderate, allowing for smaller production scales, an area fit for batch processes. Additionally, to lower investment costs and compact construction, batchwise process operation allows for close monitoring of the product quality as well as flexible and adaptive process operation. Fluctuations in the substrate composition or impurities in the feed stream can be counteracted by exploiting the additional degrees of freedom provided. Continuous processes, on the other hand, excel in production capacity and do not suffer from preparation times, leading to favorable applications in the synthesis of bulk, especially basic, chemicals. In light of transitioning from petroleum based to renewable feedstocks for chemical production, process flexibility is of great importance to handle the varying quality of raw materials. Therefore, combining the flexibility of batchwise operation with the throughput and automation of continuously operated plants should be aspired.

The focus of the present work lies on the recently introduced reactor concept of a repeated semi-batch reactor (RSBR) integrated in a continuous process for the production of n-tridecanal (nC13al) from 1-dodecene (1C12en) over hydroformylation. Kaiser et al. [1] used the methodology of *Elementary Process Functions* (EPF) [2] combined with the *Flux Profile Analysis* (FPA) approach [3] to identify optimal reactor-networks for the hydroformylation in a thermomorphic multiphase system (TMS) [4]. It was shown that integrating a semi-batch reactor (SBR) into the overall process via buffer tanks results in nearly identical performance as conventional continuous processes in terms of conversion and selectivity towards the desired product but with the additional benefit of the flexibility of a SBR. To further investigate the benefits and possible limitations of this quasi-continuous process operation, a dynamic (Dyn) model of the hydroformylation process using the RSBR and the process setup presented by Dreimann et al. [5] is developed and compared to the results of a steady-state (SS) process model as well as experimental results from a reduced

process setup.

The paper is organized as follows. At first, the configuration of the considered process is introduced in Section 3 after providing background information on the hydroformylation and discussing some previous work in this area in Section 2. Afterwards, a steady-state model is introduced in Section 4.2 which serves as a basis for comparison to the dynamic process model presented in Section 4.3. Section 5 introduces the experimental setup and summarizes the considered process conditions. In Section 6, the steady-state model is compared to the newly introduced dynamic process model. Finally, the article concludes with some final remarks in Section 7.

2. Background

The present work is part of the Collaborative Research Center TR 63 *Integrated Chemical Processes in Liquid Multiphase Systems, InPROMPT* of the German Research Foundation, a transregional cooperation with the goal to reduce the time-to-market of innovative and efficient processes. The process design is carried out with the use of renewable raw materials in mind, providing alternatives to conventional processes. In this collaboration, the major focus lies on the hydroformylation: a homogeneously catalyzed reaction used for the production of aldehydes which mainly serve as intermediate chemicals for parfume, flavour, detergent and surfactant production [6]. The demand for linear (n-) aldehydes, where the functional group is located at the end of the carbon chain, is normally higher due to better biodegradability [7]. However, even though olefins with terminal carbon-carbon double bonds are used, isomerization causes the product mixture to contain linear as well as branched (iso-) aldehydes. As a consequence, process design and control need to take the stereo- and chemo-selectivity problem into account to allow for predominant production of the desired product.

On industrial scale, hydroformylation is performed using short-chain olefins, e.g. in the Ruhrchemie-Rhône-Poulenc process [8]. Here, a biphasic catalytic system is used where the catalyst is soluble in the aqueous phase and the reactants and products are soluble in the organic phase. However, limited solubility of the reactants, including the gaseous components, in the aqueous phase pre-

vents the application of this process for long-chain olefins. As a consequence, new process concepts have to be developed utilizing e.g., alternative catalyst and/or solvent systems. With regard to the catalyst system, transition metals like cobalt and rhodium in conjunction with specialized ligands are frequently used. However, rhodium-based catalysts are generally preferred given their high activity and selectivity in this reaction [9]. As a consequence, mild process operating conditions can be used [10]. The chosen solvent system must provide adequate solubility of the components, good separability, and easy recovery of the expensive catalyst complex to ensure an economically profitable process. Walter [11] provides a good overview of different solvents including thermomorphic multicomponent solvent systems [4], micellar solvent (MLS) systems [12, 13], ionic liquids [14], gas-expanded liquids [15] and supercritical carbon dioxide [16].

When focusing on the use of TMS systems, a type III system [17] consisting of n-decane (C10an) and N-,N-dimethylformamide (DMF) as apolar and polar solvents, respectively, is generally considered for the hydroformylation of the long-chain olefin 1-dodecene [5, 18, 19, 20, 21]. Under reaction conditions, the components form a homogeneous mixture leading to the absence of transport limitations due to liquid-liquid phase boundaries. For the recovery of the catalyst, phase separation can be induced by cooling. The catalyst dissolves mainly in the polar DMF and can be recycled whereas products and unconverted reactants dissolve in the apolar phase which can be treated in subsequent downstream processing.

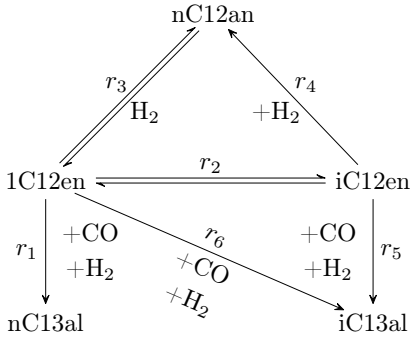

Figure 1: Reaction network adopted from Hentschel et al. [22]. 1C12en = 1-dodecene, iC12en = iso-dodecenes, nC12an = n-dodecane, nC13al = n-tridecanal, iC13al = iso-aldehydes.

This example process was already subject to multiple studies. Kiedorf et al. [19] identified the

reaction network, derived a reduced mechanistic kinetic model and parametrized it using batch experiments in which the rhodium based catalyst Rhodium-BiPhePhos with the specialized ligand BiPhePhos was employed. This kinetic model as well as the reaction network (see Figure 1) was later refined by Hentschel et al. [20] and used for dynamic optimization of a semi-batch setup to improve selectivity towards the desired linear aldehyde. In addition, Hentschel et al. [23] performed production cost optimization using the hydroformylation process of 1-dodecene augmented by downstream distillation columns for apolar solvent recovery as well as isomer separation.

In the work by McBride et al. [24], process costs were investigated with special focus on catalyst leaching. To avoid expensive calculations regarding the Liquid-Liquid-Equilibrium (LLE), a Kriging surrogate model (KR) was formulated and used in a process model with multiple extraction units to minimize the overall process costs. Kaiser et al. [25] showed a probabilistic reactor design framework which allows for quantification of uncertainties of different origin and McBride et al. [26] introduced a systematic selection of thermomorphic solvents using quantum chemical COSMO-RS calculations. Dreimann et al. [5, 21] investigated the hydroformylation process experimentally using a setup consisting of a continuously stirred tank reactor (CSTR), a liquid-liquid phase separation and different downstream processing concepts of the TMS-system for better catalyst and solvent recycling.

In a recent contribution, Kaiser et al. [1] used the FPA approach from Kaiser et al. [3] to design optimal reactor concepts for the hydroformylation miniplant, presented in Dreimann et al. [5]. They identified two reactor concepts which show promising behavior with respect to conversion and selectivity towards the linear aldehyde. Both concepts consist of two consecutive reactors and share a CSTR with synthesis gas dosing. Whereas the first process design uses a continuously operated plug flow reactor (PFR) with CO and H_2 dosing at the reactor inlet prior to the CSTR, the second concept utilizes a repeatedly operated semi-batch reactor with upstream and downstream buffer tanks. Comparison of both concepts reveals a nearly identical selectivity and conversion behavior in steady-state.

3. Process configuration

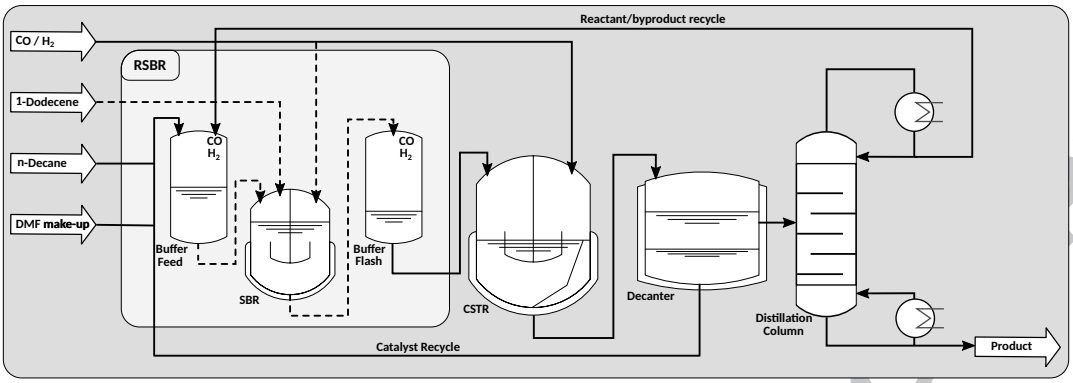

Figure 2: Simplified flowsheet of the hydroformylation process designed by Kaiser et al. [1]. Dashed lines represent periodical flows whereas solid lines symbolize continuous flows.

For better comparability, the hydroformylation process described by Kaiser et al. [1] is used as an example process. In Figure 2, the process configuration is depicted. It consists of a SBR, integrated in the continuous process via two buffer tanks – a feed buffer tank and a flash buffer tank. Following the flash buffer tank (DBuffer), a CSTR is present as a secondary reaction zone due to its beneficial back-mixing characteristics for this reaction [1]. Afterwards, the reaction mixture enters a decanter for liquid-liquid phase separation. Here, the mixture is cooled to initiate a phase split into a DMF and catalyst rich, polar phase and a (by-)product and n-decane rich, apolar phase. The apolar phase enters a subsequent distillation column where the product is separated from the apolar solvent and additional byproducts which leave the column via the distillate stream. This product depleted stream is recycled alongside the catalyst rich stream from the decanter and stored in the feed buffer tank (UBuffer) until a new process cycle can be initiated. By using additional make-up streams for the polar and apolar TMS components as well as the catalyst, constant concentrations from batch to batch are ensured. To avoid premature reaction in the feed buffer tank, the substrate 1-dodecene is injected directly into the SBR after a preparation time in each cycle.

Given the nature of the SBR which is operated with a batch time t_{B} inside of the quasi-continuous process, preparation times t_{I} for each batch are required and need to be taken into account. As

a consequence, the operation time of the continuous process needs to be equal to the sum of the preparation and batch time

$$t_{\mathrm{D}} = t_{\mathrm{I}} + t_{\mathrm{B}} \tag{1}$$

for every cycle to ensure smooth process operation.

4. Process Models

For the in-depth analysis of the RSBR-process, two process models are introduced – a steady-state and a dynamic model. Both of them share common process unit models which are summarized in Section 4.1. Afterwards, distinct features of the steady-state model as well as the dynamic model are discussed in Section 4.2 and Section 4.3, respectively. For brevity, the reaction rate, constitutive and model equations of the different process units can be found in Section A in the supplementary material. Furthermore, Section B contains the optimization problem formulations for different operating conditions of both process models alongside descriptions of the initialization strategy and overviews over process conditions and parameters.

4.1. Common Features

As both process models describe the hydroformylation reaction, all process units considered as a reaction zone rely on the same reaction network (see Figure 1) and utilize the same reaction rate equations presented by Hentschel et al. [20]. Furthermore, if gas-liquid mass transfer occurs in a process unit, the saturated gas concentration c^{sat} needs to be determined using

$$c_{\alpha}^{\mathrm{sat}} = \frac{p_{\alpha}}{H_{\alpha}}, \tag{2}$$

$$H_{\alpha} = H_{\alpha}^{0} \exp\left(\frac{-\Delta_{\mathrm{S}} H_{\alpha}}{\tilde{R}T}\right) \quad \forall \alpha \in \mathrm{GAS}, \tag{3}$$

with the corresponding Henry coefficients from Table 1.

SBR The semi-batch reactor is modeled using molar balances for the liquid as well as the gas phase . This allows for an accurate balancing of the liquid phase in the SBR as well as the dosing

Table 1: Henry coefficient parameters for hydrogen and carbon monoxide. The data is taken from Hentschel et al. [20].

i	H^0_α	$\Delta_S H_\alpha$
α	$[\mathrm{bar\,mL\,mol^{-1}}]$	$[\mathrm{J\,mol^{-1}}]$
H_2	6.64×10^4	-3.06×10^3
CO	7.39×10^4	-0.840×10^3

of gaseous components during operation. The maximum liquid hold-up is fixed to $\varepsilon_L^{SBR} = 0.66$ in accordance with Kaiser et al. [1].

CSTR In both process models the CSTR is modeled using the steady-state assumption. This assumption is also valid for the dynamic process model because of significantly lower reaction rates in comparison to the SBR. The CSTR is decoupled from the faster dynamics of the SBR due to the feed and flash buffer tanks, resulting in a nearly steady-state operation in practice. As a consequence, it is sufficient to describe the effect of backwards-isomerization of the dodecene isomers (iC12en) and the resulting increase in selectivity towards the linear aldehyde favored by the inherent back-mixing characteristics of a CSTR with a steady-state model.

The corresponding algebraic equations are used to describe the liquid phase whereas the gas phase is considered invariant in time. In contrast to the SBR where dosing of gaseous components is used to generate optimal gas phase composition profiles, the gas phase of the CSTR can be adjusted directly using the molar fraction y. This allows for maintaining the optimal partial pressures of hydrogen and carbon monoxide. As in the case of the SBR, the liquid hold-up is assumed constant and set to $\varepsilon_L^{CSTR} = 0.3$ as presented by Kaiser et al. [1].

Decanter The decanter model is a Kriging surrogate model for the liquid-liquid phase separation of the TMS-system introduced by McBride et al. [24]. It is a steady-state model which demonstrated a fast and accurate prediction of the partition coefficients of all considered species including

the catalyst ligand distribution in the polar and apolar phase. As input variables, the surrogate model requires the mole fractions of DMF, n-decane and n-tridecanal as well as the temperature of the mixture.

Distillation Column For the distillation column, a short-cut, steady-state model is used based on the Fenske-Underwood correlations which allow for the calculation of the minimum number of trays as well as the distillate and bottom streams. As in McBride et al. [24] and Kaiser et al. [1], a vacuum distillation is assumed to prevent product degradation and no pressure drop is considered. For the recovery of the light (LK $\widehat{=}$ dodecene isomers) and heavy key (HK $\widehat{=}$ n-tridecanal) in the distillate stream, $\zeta_{\mathrm{LK}}^{\mathrm{Dist}} = 0.95$ and $\zeta_{\mathrm{HK}}^{\mathrm{Dist}} = 0.05$ are used, respectively.

4.2. Steady-State Model

The steady-state process model incorporates all previously mentioned process unit models including a dedicated model for the flash buffer tank which is used for intermediately storing the reaction mixture after each batch cycle. To prevent premature liquid-liquid phase separation of the TMS-system, the buffer tank needs to maintain a temperature close to the reaction temperature [27]. Furthermore, the process unit is required to stay pressurized to retain the catalyst activity and prevent dissociation of CO from the catalyst complex [28]. As a consequence, the buffer tank needs to be considered as additional reaction zone [1]. The gas phase is not explicitly modeled because of the absence of gas dosing into the flash buffer tank. Instead, the pressure is considered constant and the gas phase composition represents the composition in the SBR at $t = t_{\mathrm{B}}$. For the steady-state model, mass balances in concentration form are used assuming a constant liquid hold-up.

In order to account for the changing outlet concentration over time due to reaction, interconnection with the subsequent CSTR is provided using the mean outlet flow

$$\dot{N}_{\alpha,\mathrm{out,mean}}^{\mathrm{DBuffer}} = \frac{1}{t_{\mathrm{D}}} \int_0^{t_{\mathrm{D}}} \dot{N}_{\alpha,\mathrm{out}}^{\mathrm{DBuffer}} \mathrm{d}t, \tag{4}$$

with t_D representing the time of one process cycle.

Instead of using a detailed model for the feed buffer tank, the initial conditions of the SBR are used to collect all recycle and make-up streams, leading to

$$n_\alpha^\mathrm{SBR}(t=0) = \int_0^{t_\mathrm{D}} \left[\left(1-\xi^\mathrm{Dec}\right) \dot{N}_{\mathrm{P},\alpha}^\mathrm{Dec} + \left(1-\xi^\mathrm{DistCol}\right) \dot{N}_{\mathrm{Dist},\alpha}^\mathrm{DistCol} + \dot{N}_{\mathrm{make-up},\alpha}^\mathrm{SBR} \right] \mathrm{d}t \quad \forall \alpha \in \mathrm{SPC} \cup \mathrm{GAS} \cup \{\mathrm{cat}\}. \tag{5}$$

Here, $\dot{N}_\mathrm{P}^\mathrm{Dec}$ and $\dot{N}_\mathrm{Dist}^\mathrm{DistCol}$ denote the polar and distillate stream of the decanter and distillation column, respectively, weighted by a corresponding purge variable ξ. Because solvent and catalyst loss occurs due to imperfect separation and the need for fresh substrate, a make-up stream $\dot{N}_\mathrm{make-up}^\mathrm{SBR}$ for the respective species is introduced. It allows for meeting additional restrictions on the initial composition and the liquid hold-up. Dreimann et al. [5] reported a ratio of $0.16 : 0.42 : 0.42\ \mathrm{wt}-\%$ of 1-dodecene to n-decane and DMF in the initial reaction mixture to ensure phase separation in the decanter. These conditions were used by Kaiser et al. [1] as well and are considered in the process model with the equality constraints

$$\left(\frac{m_\mathrm{C10an}}{m_\mathrm{DMF}}\right)^\mathrm{SBR} = \phi_\mathrm{C10an,DMF}, \tag{6}$$

$$\left(\frac{m_\mathrm{C10an}}{m_\mathrm{1C12en}}\right)^\mathrm{SBR} = \phi_\mathrm{C10an,1C12en}, \tag{7}$$

for $t_\mathrm{B} = 0$. Additionally, the ratio of catalyst metal to substrate is constrained to $\phi_\mathrm{cat,1C12en} = {}^1/_{4000}$ [1, 5] using

$$\left(\frac{n_\mathrm{cat}^\mathrm{SBR}}{n_\mathrm{1C12en}}\right)(t_\mathrm{B}=0) = \phi_\mathrm{cat,1C12en}. \tag{8}$$

To prevent an overfilling of the SBR and to ensure correct pressure levels, the liquid hold-up is restricted via

$$0 = V^\mathrm{SBR}\varepsilon_\mathrm{L}^\mathrm{SBR} - V_\mathrm{L}^\mathrm{SBR}(t=0). \tag{9}$$

In contrast to the steady-state model by Kaiser et al. [1] where the SBR and the flash buffer tank are considered as one unit with a combined residence time $t_{\mathrm{SBR+DBuffer}}$, the SBR and flash buffer tank are modeled as two separate process units. Therefore, the residence time needs to be distributed between them, leading to

$$0 = \tau_{\mathrm{DBuffer}} + t_{\mathrm{B}} - t_{\mathrm{SBR+DBuffer}}, \tag{10}$$

$$\tag{11}$$

with the batch time t_{B} and the residence time of the flash buffer tank defined as

$$\tau_{\mathrm{DBuffer}} = \frac{V_{\mathrm{L}}^{\mathrm{SBR}}(t = t_{\mathrm{B}})}{\dot{V}_{\mathrm{out}}}. \tag{12}$$

The formulation of the steady-state process model in the form of an optimization problem maximizing the selectivity towards the linear aldehyde is denoted as DOP1 or DOP2, depending on the process parameters.

4.3. Dynamic Process Model

One major drawback of the previously introduced steady-state model is the limitation on the prediction of the cyclic steady-state – a state in which the dynamic profiles of each process unit stay constant over an unspecified number of batch cycles. Variations of the liquid hold-up in each process unit as well as fluctuations which occur during process start-up or as a consequence of external disturbances cannot be described. Furthermore, introducing a non-continuous process unit in a continuous overall process requires a strategy for the interaction between both parts. In the previously described process setup (see Section 3 and Figure 2), continuous operation is achieved by the use of two buffer tanks, one before and one after the semi-batch reactor. Nonetheless, filling and emptying of the SBR always represent discrete events which need to be accounted for in the process model. In the case of the steady-state model, assumptions and simplifications are made in order to integrate the SBR into the continuous process model. In the case of a dynamic process

model, consideration of the time allows for rigorous modeling of each process unit without the need for major assumptions.

In the following, the dynamic process model is introduced. For the sake of a concise overview, the main aspects of each process unit model specific to the dynamic formulation is outlined and additional process relevant limitations are discussed. Afterwards, the methodical approach for the interconnection of the non-continuous and continuous parts of the process is presented. Detailed information on the process unit models can be found in Section A of the supplementary materials.

4.3.1. Unit Models

Flash Buffer Tank The dynamic behavior of the flash buffer tank can be expressed using Ordinary Differential Equations (ODEs) for all species in the liquid phase and the catalyst. The gas phase is not explicitly modeled because of the absence of gas dosing into the flash buffer tank. Similar to the SBR, the flash buffer tank is modeled using molar balances in order to track the liquid content which is depleted over one process cycle to a residual liquid hold-up $V_{\mathrm{L,min}}$. For an accurate description of the reaction activity in the buffer tank, changes in pressure are approximated as ideal at isothermal conditions. As a consequence, a decreasing liquid hold-up leads to a decrease in the overall pressure resulting in reduced gas-liquid mass transfer.

Feed Buffer Tank Both recycle streams and the make-up stream are fed to the feed buffer tank which stores the reaction mixture until the next process cycle. Due to the absence of significant amounts of substrate, missing gas-liquid mixing and the low pressure, the feed buffer tank is not assumed to be a reaction zone, hence no source term is considered. However, gas-liquid mass transfer is included in the model, allowing for a more accurate representation of the conditions at the beginning of each batch cycle where mass transfer limitations would otherwise determine the rate of reaction. Similar to the flash buffer tank, the pressure in the feed buffer tank is not considered constant but varies with the liquid hold-up.

4.3.2. Methodical Approach

The dynamic description of a RSBR-process requires careful modeling of the interconnections of each process unit and attention to the solution procedure due to non-smoothness of the state variables as well as strong nonlinearities in each process unit. In Figure 3, the concentration profiles

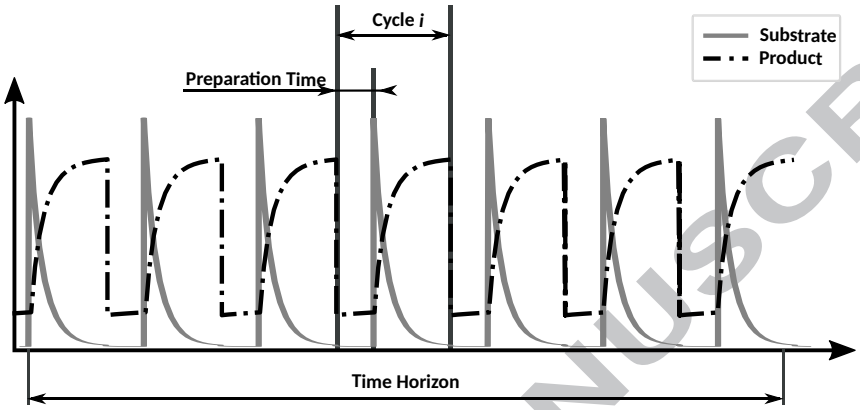

Figure 3: Concentration profiles of a general RSBR-process.

of a repeated semi-batch reaction is illustrated indicating the intermittent dosing of substrate and the cyclic formation of product. Here, the time horizon can be subdivided into process cycles which in turn consist of a preparation and reaction phase. It is apparent that the beginning and end of each cycle is marked by significant differences in product concentration due to emptying and refilling of the SBR. This combination of discrete decisions and dynamics is generally denoted as hybrid dynamics [29] and may lead to non-smoothness in the parameter sensitivities if no special care is taken in the case of discretization in time [30]. This is especially important for process optimization using the dynamic process model since reformulation of the dynamic optimization problem (DOP) as a nonlinear program (NLP) by discretization in time is a common approach. There are multiple ways to formulate the RSBR-process as an optimization problem, e.g., by using integer variables for the logical decisions leading to a mixed-integer dynamic optimization problem (MIDO) [31], by using Generalized Disjunctive Programming to form mixed logic dynamic optimization problems [32] or by reformulating the logical decisions via smoothing constraints or complementarity constraints [30].

Formulation as a MIDO generally leads to a NP-hard optimization problem which may become expensive to solve for fine discretization in time [30]. On the other hand, reformulation using complementarity constraints is non-trivial and requires great care in problem formulation and with respect to the solution strategy [33]. Due to the sequential nature of the RSBR-process, a cycle-based problem formulation can be chosen, leading to a DOP. As a consequence, non-smooth changes in the species concentrations are avoided at the beginning of each new process cycle by subdividing the optimization problem into process cycles as shown in Figure 3. Simulation and optimization of the full time horizon is achieved by repeatedly solving the dynamic process model using the final concentrations and the liquid hold-up in the feed buffer tank of the respective previous cycle as initial conditions for the SBR. This cycle-based approach has the advantage of reducing the size of the resulting optimization problem significantly. As downside, it complicates the formulation of process targets which lie ahead of the current process cycle, e.g., reaching a specific product yield after a predefined number of process cycles.

When focusing on one process cycle, two intervals can be distinguished. One interval with negligible changes in substrate and product concentration and one interval with pronounced concentration profiles, both separated by a sudden increase in substrate concentration. The first interval represents the preparation phase in which the SBR is emptied and refilled, whereas the second interval indicates reaction activity initiated by dosing of fresh substrate. Even though substrate dosing can be modeled by specifying a control trajectory or by using constraints, non-smoothness of the substrate concentration profile may lead to numerical difficulties and convergence problems. Therefore, the interval of each process cycle is divided again into two subintervals and a separate SBR model is assigned to each interval.

Figure 4 illustrates the separation of the preparation or *Idle* stage from the *Reaction* stage in each process cycle. Furthermore, a *Continuous* stage is introduced which contains the continuously operated process units, i.e., buffer tanks, CSTR, decanter and distillation column. At this point, it is necessary to introduce a convention for counting the process cycles. In the remainder of the article, the process cycles are counted based on the reaction mixture. For example, the

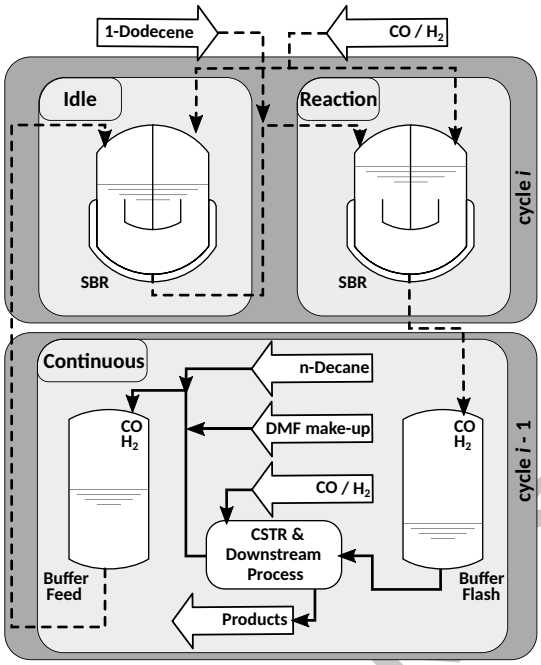

Figure 4: Cycle-based process simulation and optimization work flow (dashed lines periodically flow; solid lines continuously flow).

reaction mixture of cycle i is processed in the *Idle* and *Reaction* stage while the *Continuous* stage simultaneously operates with the reaction mixture of cycle $i-1$.

4.3.3. Process Model Formulation

The proposed process model consists of two optimization problems which are solved in sequence for each process cycle. The first optimization problem contains the *Idle* stage whereas the second optimization problem combines the *Reaction* and *Continuous* stage. This decoupling is possible due the minor influence of the first stage and leads to a reduced problem size of the resulting NLP as well as a simplified solution procedure. However, it is not required for applying the described process formulation. For instance, interconnection of two process units which are operated sequentially, e.g., a SBR and a buffer tank, can be accomplished by manually assigning the numerical values of the final states of one unit as initial conditions to the subsequent unit or by connecting both via linking constrains of the respective state variables. In the following, the separate optimization

problems are discussed in more detail.

In the *Idle* stage, the SBR model is solved for cycle i over the preparation time t_I according to DOP4. As initial conditions, the liquid hold-up and the concentrations of the feed buffer tank from cycle $i-1$ are used. Since substrate dosing does not occur in the preparation stage and only minor reaction activity is observable due to dodecene isomers and traces of 1-dodecene in the recycle streams, the influence of optimal control of the gas dosing on the selectivity towards the desired product is negligible. As a consequence, it is sufficient to perform an integration of the underlying Differential-Algebraic system (DAE).

The *Reaction* stage and the *Continuous* stage are solved as one optimization problem according to DOP5 or DOP6, depending on the process setup. They are connected by using equality constraints of the form

$$0 = n_\alpha^{\mathrm{SBR}}(t = t_\mathrm{B}) - n_\alpha^{\mathrm{DBuffer}}(t = 0) \quad \forall \alpha \in \mathrm{SPC} \cup \mathrm{GAS}, \tag{13}$$

$$0 = n_{\mathrm{cat}}^{\mathrm{SBR}} - n_{\mathrm{cat}}^{\mathrm{DBuffer}}(t = 0), \tag{14}$$

$$0 = y_\alpha^{\mathrm{SBR}}(t = t_\mathrm{B}) - y_\alpha^{\mathrm{DBuffer}}(t) \quad \forall \alpha \in \mathrm{GAS}, \tag{15}$$

for linking the state variables of the SBR at t_B to the initial conditions of the flash buffer tank. Following the previously introduced convention of the process cycles, the reaction mixture of cycle i from the previously solved *Idle* stage is enriched by fresh substrate and used for the initial conditions of the *Reaction* and *Continuous* stage. As discussed in Section 4.2, restrictions on the composition of the reaction mixture and the maximum liquid hold-up in the SBR have to be considered to ensure phase separation of the TMS in the decanter. Due to the cycle-based formulation of the process model, these restrictions apply for the SBR in cycle $i+1$ even though the make-up streams for the catalyst, solvents and fresh substrate which are able to influence the composition of the reaction mixture in cycle $i+1$ are available in cycle i. As a consequence, these restrictions need to be reformulated as constrains for cycle i to ensure that the control variables and the constrains are considered in the same optimization problem. Since the final conditions at

t_D of the feed buffer tank in cycle i are equal to the initial conditions of the SBR in the *Idle* stage of cycle $i+1$, the constrains can be formulated for the feed buffer tank instead, leading to

$$\left(\frac{m_\mathrm{C10an}}{m_\mathrm{DMF}}\right)^\mathrm{UBuffer}(t_\mathrm{D}) = \phi_\mathrm{C10an,DMF}, \tag{16}$$

$$\left(\frac{m_\mathrm{C10an}^\mathrm{UBuffer}(t_\mathrm{D})}{m_\mathrm{1C12en}^\mathrm{UBuffer}(t_\mathrm{D}) + m_\mathrm{1C12en,fresh}^\mathrm{SBR}}\right) = \phi_\mathrm{C10an,1C12en}, \tag{17}$$

to ensure the correct ratio of polar solvent, apolar solvent and fresh 1-dodecene. Furthermore, any loss of catalyst due to imperfect separation in the decanter needs to be compensated using

$$\frac{n_\mathrm{cat}^\mathrm{UBuffer}(t_\mathrm{D})}{n_\mathrm{1C12en}} = \phi_\mathrm{cat,1C12en}, \tag{18}$$

and the liquid hold-up in the SBR is limited via

$$0 = V_\mathrm{L}^\mathrm{UBuffer}(t_\mathrm{D}) + V_\mathrm{1C12en,fresh} - V^\mathrm{SBR}\varepsilon_\mathrm{L}^\mathrm{SBR}. \tag{19}$$

To summarize, the problem can be represented as a set of optimization problems DOP4 and DOP5 or DOP6, respectively. Since no optimal gas dosing is considered in the *Idle* stage, the problem can be formulated as a DOP with the objective function set to zero. The combined solution of the *Reaction* and *Continuous* stage can also be represented as a DOP with the objective function containing a weighted combination of maximizing the selectivity towards the linear aldehyde and emptying of the flash buffer tank to a predefined liquid hold-up over the time horizon t_D of one process cycle. The *Idle* stage and the combination of *Reaction* and *Continuous* stage are solved in sequence, so that the repeated operation of the SBR is simulated dynamically. The process can be summarized with the following algorithm.

Solution Procedure

Given: Initial liquid content n_0^{SBR}, catalyst amount $n_{\mathrm{cat},0}^{\mathrm{SBR}}$, temperature T_0^{SBR}, pressure p_0^{SBR} and gas phase composition y_0^{SBR} of the *Reaction* stage; cycle $i \in [0, \infty)$; $cycles_{\max} \in [2, \infty)$; $t_{\mathrm{I}}, t_{\mathrm{B}}, t_{\mathrm{D}} \in [0, \infty)$.

1) *Initialize and solve the Reaction and Continuous stage.* Initialize the iteration counter $i \leftarrow 0$. Solve the *Reaction* stage over the batch time t_{B} and the *Continuous* stage over the time horizon of the downstream process $t_{\mathrm{D}} = t_{\mathrm{B}} + t_{\mathrm{I}}$.

2) *Initialize the Idle stage.* Set $n^{\mathrm{SBR,idle}}(t = 0) \leftarrow n^{\mathrm{UBuffer}}(t = t_{\mathrm{D}})$, $n_{\mathrm{cat}}^{\mathrm{SBR,idle}} \leftarrow n_{\mathrm{cat}}^{\mathrm{UBuffer}}(t = t_{\mathrm{D}})$.

3) *Initialize and solve the Reaction and Continuous stage.* Since the recycle is not yet available, set $n^{\mathrm{SBR}}(t = 0) \leftarrow n_0^{\mathrm{SBR}}$, $n_{\mathrm{cat}}^{\mathrm{SBR}} \leftarrow n_{\mathrm{cat},0}^{\mathrm{SBR}}$, $T^{\mathrm{SBR}} \leftarrow T_0^{\mathrm{SBR}}$, $p^{\mathrm{SBR}} \leftarrow p_0^{\mathrm{SBR}}$ and $y^{\mathrm{SBR}} \leftarrow y_0^{\mathrm{SBR}}$. Increment the counter $i = i + 1$ and solve.

4) *Solve the Idle stage.* Update the counter $i \leftarrow i + 1$ and solve over the preparation time t_{I}.

5) *Initialize the Reaction and Continuous stage.* Set $n^{\mathrm{SBR}}(t = 0) \leftarrow n^{\mathrm{SBR,idle}}(t = t_{\mathrm{I}}) + n_{\mathrm{fresh}}^{\mathrm{SBR}}$, $n_{\mathrm{cat}}^{\mathrm{SBR}} \leftarrow n_{\mathrm{cat}}^{\mathrm{SBR,idle}}$, $T^{\mathrm{SBR}} \leftarrow T_0^{\mathrm{SBR}}$, $p^{\mathrm{SBR}} \leftarrow p_0^{\mathrm{SBR}}$ and $y^{\mathrm{SBR}} \leftarrow y_0^{\mathrm{SBR}}$.

6) *Initialize the Idle stage.* Set $n^{\mathrm{SBR,idle}}(t = 0) \leftarrow n^{\mathrm{UBuffer}}(t = t_{\mathrm{D}})$, $n_{\mathrm{cat}}^{\mathrm{SBR,idle}} \leftarrow n_{\mathrm{cat}}^{\mathrm{UBuffer}}(t = t_{\mathrm{D}})$.

7) *Solve the Reaction and Continuous stage.* If $i \geq cycles_{\max}$, then STOP, else continue at 4).

5. Experimental Setup

For testing the feasibility of the quasi-continuous process operation and the predictions made by the steady-state and dynamic process model, experiments are prepared under miniplant conditions.

A reduced process setup, depicted in Figure 5, is employed neglecting the apolar recycle from the distillation column (compare Figure 2). Table 2 and Table 3 provide a list of equipment

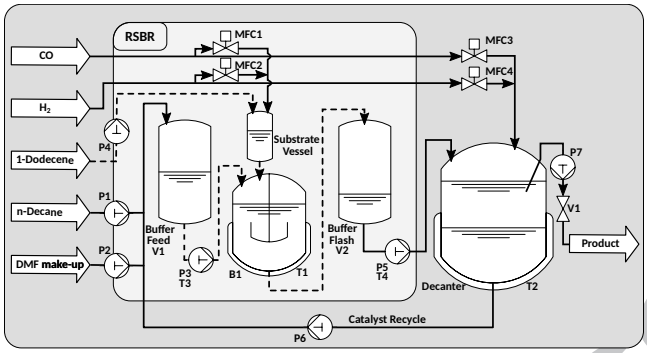

Figure 5: Simplified flowsheet of the experimental setup.

and chemicals, respectively, which were used in the miniplant setup and Table 4 summarizes the experimental conditions.

Every new batch is initiated by pressurizing the substrate vessel with synthesis gas to 23 bar. The gas flow is regulated by the mass flow controllers MFC1 and MFC2 for CO and H_2, respectively, which are controlled by the process control system (PCS) of the RSBR-rig (feed and flash buffer tank, SBR). Subsequently, the ball valve to the reactor is opened, and the substrate is injected into the SBR with a pressure difference of approximately 9 bar.

During the reaction, the temperature inside the reactor is dynamically controlled by a thermostat T1 and synthesis gas is constantly fed into the reactor to maintain the pressure level. After passing the reaction time, the gas flow is stopped and the valves between the reactor and flash buffer vessel opened to transfer the reaction mixture via pressure differences. To ensure complete emptying of the SBR, the reactor is pressurized and depressurized into the flash buffer vessel several times. Subsequently, the reactor is filled with the mixture from the feed buffer vessel for the next batch cycle.

The continuous part of the experimental setup includes the decanter with temperature control via thermostat T2 and pressure control via the mass flow controllers MFC3 and MFC4. It needs to be mentioned, that the decanter vessel did not contain any installations inside for enhancing the

Table 2: Experimental equipment.

Manufacturer	**Type**	**ID**
KNAUER Wissenschaftliche Geräte GmbH	Smartline 1000	P3*
	Smartline 1050	P1, P4, P5*, P7
	AZURA P4.1S	P2, P6
Büchi AG	Miniclave 240 mL	B1
	Vesoclave type 4, 1 L	D1**
Julabo GmbH	FP40HL	T1, T3, T4
	F32	T2
Brooks® Instrument	Series SLA5800	MFC1, MFC2, MFC3, MFC4
Swagelok®	R-Series 1'-fittings	V1 V2, V3
Agilent	9820 gas chromatograph	-
	HP5-column	-
	FID detector	-
Siemens	PCS7 V.8.1	-

* Pump heads are heated and connected to T3 and T4, respectively. ** Without additional installations.

Table 3: Chemicals supplier and purity.

Manufacturer	**Chemical**	**purity**
Merck	n-Decane	$> 99\,\%$
Sigma-Aldrich®	DMF	$> 99\,\%$
	Rh-precursor	$> 98\,\%$
Molisa	BiPhePhos	$> 99\,\%$
Alfa Aesar®	1-Dodecene	$> 97\,\%$

Table 4: Process conditions of the experimental setup.

	Parameter	[.]	Value
SBR	T	°C	105
	p	bar	19
	y_{H_2}/y_{CO}	−	1
DBuffer	T	°C	91
	p_0	bar	16.21
	y_{H_2}/y_{CO}	−	1
Dec	T	°C	5

	Parameter	[.]	Value
UBuffer	T	°C	96
	p_0	bar	2.875
	y_{H_2}/y_{CO}	−	1
Process	t_I	min	30
	t_B	min	60
	$\phi_{C10an,DMF}$	$g\,g^{-1}$	1
	$\phi_{C10an,1C12en}$	$g\,g^{-1}$	$^{42}/_{16}$
	$\phi_{cat,1C12en}$	$mol\,mol^{-1}$	$^{1}/_{224}$

phase separation. The product phase is removed from the decanter using an immersion tube at the top, connected to pump P7 and relief valve V1 for overcoming the pressure difference of 23 bar between the decanter and the atmospheric product vessel. The catalyst phase, on the other hand, is continuously fed into the feed buffer tank using pump P6.

As previously mentioned, the process is controlled by two separate process control systems, one for the RSBR-rig and one for the decanter as well as the feed pumps. To prevent phase separation of the TMS-system inside of the pipelines between the vessels and the buffer vessels, electric heating ducts are wrapped around the tubes. This also includes the pump heads of P3 and P5 where temperature is controlled by thermostats T3 and T4, respectively. Information on the liquid hold-up in the buffer tanks was available using sight glasses.

Multiple liquid samples were taken per batch from the SBR in predefined intervals for analysis. Each sample was diluted immediately with 2-propanol to prevent phase separation at room temperature and the composition was determined using gas chromatography (GC).

6. Results and Discussion

In the following, simulation results from both process models as well as the experimental results are discussed. The remainder of this section is organized as follows. After validation of the steady-state process model (see Section C of the supplementary materials), the dynamic process model is compared to the steady-state model to verify its integrity and to show additional aspects of the process which are not described by the steady-state model. Subsequently, the dynamic model is used to predict the process behavior resolved in time to compare to the composition profile taken from the experimental samples in cyclic steady-state.

All process model equations are implemented in the toolbox for gradient-based numerical optimization CasADI 3.3 [34] using the API to Python 3.6.6 [35]. The DOPs are reformulated as Nonlinear Programs (NLPs) using direct collocation on 20 finite elements with 3 collocation points before solving the resulting algebraic equations using the Interior Point OPTimizer IPOPT 3.12.3 [36] together with the linear solver MA27 [37]. To prevent numerical issues and to ensure conver-

gence of the optimization algorithm, variable scaling is implemented alongside specialized initialization strategies for both process models. The steady-state model is initialized with integration results, solved in approximately 19 s without taking into account the recycle streams and finally computed with all recycle streams enabled in 32 s. In the case of the cycle-based calculation of the dynamic process model, each process cycle contains multiple initialization steps before the full process model is solved. At first, the state and control trajectories for the batch reactor are calculated without taking into account the CSTR and the downstream process. Using these results as a first initialization, the complete process model is integrated and reinitialized before solving the NLP. The calculation time depends on the process cycle and ranges from 42 s for the first to 11 s for process cycles in cyclic steady-state. On average 15 s are required for the initialization and calculation of one process cycle. All calculations were performed on a machine with an Intel® Core™ i5-7200U with 8 GB of RAM.

6.1. Comparison of the steady-state and dynamic model

After validating the steady-state model it can be used to asses the results of the dynamic model. For the comparison of both models, an operating point is specified which takes into account the specifications of the experimental equipment. They differ from the specifications presented by Kaiser et al. [1] which is especially relevant in the case of the residence time, the volume of the SBR (specified: 550 mL, reality: 240 mL) and buffer tank vessels. Minor differences are related to the flash buffer tank which is kept at a constant temperature of 91 °C to prevent premature phase separation and a reduced pressure of maximal 16.21 bar after transferring of the reaction mixture from the SBR. In the course of one process cycle, the flash buffer tank is not emptied completely but a residual liquid hold-up of $V_{\mathrm{L,min}}^{\mathrm{DBuffer}} \approx 25\,\mathrm{mL}$ is kept in the vessel, leading to a volumetric flow rate of

$$\dot{V}_{\mathrm{out}} = \frac{V_{\mathrm{L}}^{\mathrm{DBuffer}}(t=0) - V_{\mathrm{L,min}}^{\mathrm{DBuffer}}}{t_{\mathrm{D}}} \tag{20}$$

at the outlet. For easier process operation, the batch time is kept constant at 60 min with a preparation time of 30 min for each new batch. For the CSTR and distillation column, the operating conditions are chosen according to Kaiser et al. [1].

Under consideration of the restrictions summarized in Table B.1, B.3 and B.4, DOP2 as well as DOP4 and DOP5 are solved for the steady-state and dynamic process model, respectively. In Figure 6a, the selectivity - conversion behavior is depicted over the considered time horizon of

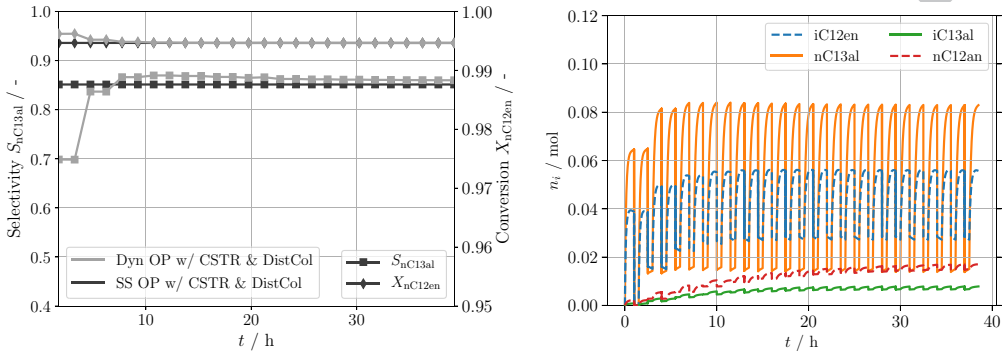

(a) Selectivity-conversion behavior.

(b) Dynamic composition profiles of the dynamic process model.

Figure 6: Comparison of the steady-state model using the *SS w/ CSTR & DistCol* case (DOP2) and the dynamic model w/ CSTR and distillation column (DOP4 and DOP5). A comparison of the composition profiles of both process model in cyclic steady-state can be found in Section D of the supplementary materials.

25 cycles for the dynamic process model. For better comparability, the selectivity and conversion of the steady-state model is added as constant values over time. Due to the absence of a recycle stream from the distillation column in the first two cycles of the dynamic consideration, the selectivity towards the linear aldehyde is limited to 69.85 % while the conversion is at its maximum with 99.62 %. Following the principle of Le Chatelier, the recycle of dodecene isomers reduces 1-dodecene isomerization and leads to a significant increase in selectivity with a minor decrease in conversion. After approximately seven process cycles, fluctuations diminish and the selectivity and conversion converge to stable values of 86.00 % and 99.47 %, respectively. With a selectivity of 85.23 %, the

steady-state model exhibits a minor difference of 0.77 % at an identical conversion.

When taking a closer look at the composition profiles in Figure 6b, the isomer recycle is clearly visible after the first two process cycles. The amount of recycled dodecene isomers increases in the first eight cycles until reaching a cyclic steady-state. The minor decrease in concentration during the *Idle* stage is due to residual backwards-isomerization and hydroformylation. This reaction activity is mirrored by the increase in tridecanal production. Since the polarity of both, linear and branched, aldehydes increases in comparison to their respective olefins, the amount of hydroformylation product in the polar recycle stream increases as well, leading to a significant initial concentration at the beginning of each process cycle. Another important species for the start-up behavior of the RSBR-process is the hydrogenation product n-dodecane. Even though all dodecene isomers and the different hydroformylation products reach recurring composition profiles after approximately eight process cycles, n-dodecane converges to a stable concentration after more than twice as many process cycles and therefore determines the time required for the entire process to reach a cyclic steady-state. The formation of n-dodecane is strongly related to the hydrogen content in the gas-phase of the SBR and CSTR and therefore directly influenced by the dosing of hydrogen and carbon monoxide. The solver needs to determine $j_{\mathrm{H_2}}^{\mathrm{SBR}}$ and $j_{\mathrm{CO}}^{\mathrm{SBR}}$ to maximize selectivity towards the linear aldehyde while simultaneously minimizing the deviation from the desired terminal liquid hold-up of the flash buffer tank and ensuring Eq. (16-19). As a consequence, convergence of the RSBR-process to an optimal cyclic steady-state not only requires accurate knowledge of the underlying reaction network but also precise control of the reaction conditions.

To summarize, both process models deliver coinciding predictions of the compositions and process performance in cyclic steady-state. Despite its reduced process unit model complexity, the steady-state model allows for an accurate depiction of the process behavior while showing advantages with respect to process model complexity and computation time. The dynamic process model, on the other hand, enables the resolution of the process dynamics including its start-up behavior. As a consequence, valuable information, e.g. the start-up time, can be estimated and used for planning of the experimental investigation. Furthermore, the availability of a dynamic process model allows

for the application of on-line process control, e.g., by the use of nonlinear model predictive control.

6.2. Comparison with experimental data

In the previous section, convergence of both process models to the same cyclic steady-state has been shown. Therefore, the concentration profiles of the SBR predicted by the dynamic model can be used for comparison to the experimentally determined profiles.

The experiments were conducted using the process parameters summarized in Table 4. Due to the frequent change of pressure in the buffer vessels, deactivation of the catalyst by CO desorption from the active site was expected [9]. To counteract the degradation of reactivity, a higher catalyst concentration was used to demonstrate the feasibility of the process setup. In Figure 7, experimental and simulated mass fraction profiles of the major species are shown for the cyclic steady-state of the SBR. The computations were performed using DOP4 and DOP6 with the process parameters from Table B.4 and Table 4 for a reduced process configuration without the CSTR and distillation column. Due to gas dosing being limited to synthesis gas (equal amount of hydrogen and carbon monoxide) in the experimental setup,

$$j_{\mathrm{CO}}^{\mathrm{SBR}}(t) - j_{\mathrm{H_2}}^{\mathrm{SBR}}(t) = 0, \tag{21}$$

is added to DOP6. Furthermore, the number of process cycles is limited to 10 because of the fast convergence to the cyclic steady-state exhibited for the reduced process configuration without dodecene isomer recycle.

Overall, the calculated concentration profiles show a qualitative agreement with the experimental data. Due to the increased catalyst concentration, two reaction sections can be distinguished. In the first section, the fresh 1-dodecene added at the beginning of each batch cycle immediately isomerizes and reacts via r_1 to the linear aldehyde, leading to a spike in the concentration of these two species. In the second section, the previously formed dodecene isomers undergo backwards-isomerization to 1-dodecene and subsequently react to the desired product. Due to the backwards-isomerization being the rate determining step, the slope of the concentration profiles is significantly

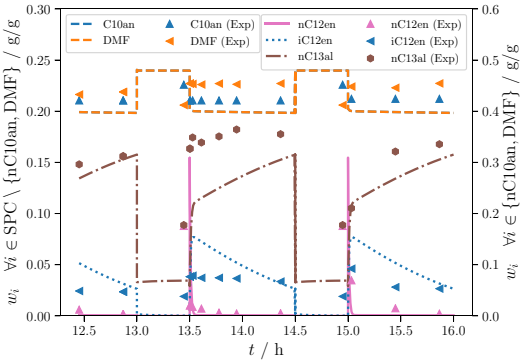

Figure 7: Experimental and simulated cyclic steady-state compositions in the SBR using the dynamic process model.

reduced in comparison to the first section.

When comparing the predicted and measured concentration profiles of the dodecene isomers and the linear aldehyde, deviations in the trajectory can be observed. Even though the data shows good agreement at the beginning and the end of each cycle, the experimental results indicate a faster backwards-isomerization of the dodecene isomers. As a consequence, the overall reaction rate towards the linear aldehyde increases, leading to significantly higher tridecanal concentrations early in the batch cycle. It is concluded that the reaction rate expressions and parameters which were estimated using a catalyst metal to substrate ration of $^1/_{10000}$ [20] are not applicable for the present process conditions in terms of depicting the reaction dynamics. Even though the catalyst concentration is contained in the reaction rate expressions, no study was performed on the influence of changing catalyst concentrations on the reaction kinetics. Nevertheless, predicted and measured concentrations converge to comparable values at the end of each cycle, allowing for integral predictions of the state of the system.

Possible explanations for the deviations from the experimental solvent concentrations involve an incomplete liquid-liquid phase separation as well as experimental limitations on the real-time measurements of the liquid phase composition. As already discussed in Section 5, the decanter vessel did not contain installations for enhancing phase separation. As a consequence, mixing effects of the polar and apolar phase due to the inlet stream are possible, leading to short-cut

streams inside of the decanter. An increased concentration of apolar components in the catalyst recycle stream leads to an offset of the solvent concentration if the make-up streams and the dosing of fresh substrate are not adjusted accordingly. Because of the absence of real-time composition measurements, e.g., via spectroscopic methods, these adjustments could not be made, resulting in the observed deviations.

Despite the deviations between the model predictions and the experimental data, the model proofed its ability to predict the process performance in a qualitative manner. Furthermore, the experimental proof-of-concept of integrating a cyclically operated semi-batch reactor in a continuous process for the hydroformylation of long-chain olefins is provided.

7. Conclusion

Based on the process design by Kaiser et al. [1] for the hydroformylation of 1-dodecene in a n-decane/DMF TMS-system, a dynamic process model has been developed. By dividing the process into two stages and performing separate cycle-based optimizations of each stage sequentially, a repeated semi-batch process is simulated which allows for the investigation of non-stationary process states, e.g., process start-up.

For the validation of the dynamic process model, a steady-state model has been formulated and validated in accordance with Kaiser et al. [1]. By comparing the composition profiles and the process performance via the conversion of 1-dodecene and the selectivity towards the desired linear aldehyde tridecanal, the integrity of the dynamic process model is shown. Furthermore, an estimate for the start-up time of the RSBR-process is given by considering the time required for the convergence of all species compositions to their respective steady-state value.

In addition to the theoretical investigation of the RSBR-process, the practical feasibility is assessed by performing experiments in a reduced process setup which consists of the SBR, two buffer tanks and a decanter for catalyst recovery. Comparison of the concentration profiles indicates good agreement of initial and final concentrations of the main species in each batch cycle, resulting in a qualitative description of the overall process behavior. For an improved prediction of the

dynamic process behavior for high catalyst concentrations, estimation of the reaction kinetics in an extended operating window is one possible aspect for future work.

To summarize, the formulation of dynamic process models for the repeated operation of a semi-batch reactor in a continuous process has been exemplified for the hydroformylation of 1-dodecene in a thermomorphic multiphase system. Besides the validation of the dynamic process model using a steady-state model, the practical feasibility of the process is investigated in miniplant scale. The collected data reveals a qualitative agreement of simulated and experimental results.

In a next step, the RSBR-rig will be extended by a CSTR to realize the optimal reactor network proposed by Kaiser et al. [1]. For this, the presented dynamic process model will be of great help to predict the performance and to support the design of experiments. With a quantitative agreement of experiments and simulations, possible directions for future work would include the application of the dynamic process model in model predictive control. Furthermore, the application of the process design methodology of Kaiser et al. [1] to other example reactions and process scales should be pursued which may lead to additional occurrences of repeated semi-batch reactor concepts.

Acknowledgment

This work is part of the Collaborative Research Center/Transregio 63 „Integrated Chemical Processes in Liquid Multiphase Systems“ (subproject B1). Financial support by the Deutsche Forschungsgemeinschaft (DFG, German Research Foundation) is gratefully acknowledged (TRR 63). The author Karsten H. G. Rätze is also affiliated to the „International Max Planck Research School (IMPRS) for Advanced Methods in Process and Systems Engineering (Magdeburg)“. Furthermore, the authors would like to thank Markus Ikert, Claudia Bednarz, Patrick Siegmund, Stefanie Markstein, Melanie Fachet and Ali ElSibai for their support in the experimental investigations.

Nomenclature

Abbreviations

acac Acetylacetonato

BiPhePhos 6,6′[(3,3′-Di-tert-butyl-5,5′ -dimehtoxy-1,1′-biphenyl-2,2′diyl) bis(oxy)]bis(dibenzo[d,f][1,3,2] dioxaphosphepin

CasADI Software name

cat Catalyst

COSMO-RS Conductor like screening Model for Real Solvents (software name)

nC12an n-Dodecane

DAE Differential-Algebraic System

1C12en 1-Dodecene

iC12en Dodecene isomers

C10an n-Decane

DMF N,N-Dimethylformamide

DOP Dynamic Optimization Problem

Dyn Dynamic

EPF Elementary Process Functions

Exp Experimental

FPA Flux Profile Analysis

GC Gas Chromatography

iC13al Isomeric Aldehydes

IPOPT Interior Point OPTimizer (software name)

Init Initial

KR Kriging model

LB Lower Bound

LLE Liquid-Liquid Equilibrium

MA27 Linear solver from the HSL Mathematical Software Library

MFC Mass flow controller

MIDO Mixed-Integer Dynamic Optimization Problem

NLP Nonlinear Program

ODE Ordinary Differential Equation

PCS Process Control System

PFR Plug flow reactor

r Reaction

RSBR Repeated semi-batch reactor

SBR Semi-batch reactor

SS Steady-state

nC13al Tridecanal

TMS Thermomorphic Multiphase System

UB Upper Bound

wt weight

Sets

GAS H_2, CO

RCT Set of reactions r_1 to r_6

SPC C10an, DMF, 1C12en, iC12en, nC13al, iC13al, nC12an

UBufferInput Input streams to the feed buffer tank

Greek symbols

α	Relative volatility	$[\mathrm{mol\,mol^{-1}}]$
$\overline{\alpha}$	Mean relative volatility	$[\mathrm{mol\,mol^{-1}}]$
Δ	Difference	
ε	Hold-up	$[\mathrm{mL\,mL^{-1}}]$
η	Recovery in a distillation column	[–]
ζ	recovery	$[\mathrm{mol\,mol^{-1}}]$
θ	Partition coefficient	$[\mathrm{mol\,mol^{-1}}]$
ν	Stoichiometric coefficient	[–]

ξ	purge	$[\mathrm{mol\,mol^{-1}}]$
ρ	Mass density	$[\mathrm{kg\,m^{-3}}]$
τ	Residence time	[s]
φ	Helping variable for residence time calculation	$[\mathrm{L\,L^{-1}}]$
ϕ	Mass or mole ratio	[g/g, mol/mol]

Latin symbols

a, a_ρ	Various parameters	[various]
c	Concentration	$[\mathrm{mol\,mL^{-1}}]$
E_A	Activation Energy	$[\mathrm{J\,mol^{-1}}]$
ΔG	Gibbs energy of reaction	$[\mathrm{J\,mol^{-1}}]$
H	Henry coefficient	$[\mathrm{bar\,mL^{-1}\,mol^{-1}}]$
$\Delta_\mathrm{S} H$	Enthalpy of solution	$[\mathrm{J\,mol^{-1}}]$
j	Dosing stream	$[\mathrm{mol\,s^{-1}}]$
k	Reaction rate coefficient	[various]
K, K_p	Equilibrium constant	[various]
$k_\mathrm{L}a$	Volumetric mass transfer coefficient	$[\mathrm{min^{-1}}]$
$\tilde{M}$	Molar mass	$[\mathrm{kg\,mol^{-1}}]$
m	Mass	[kg]

$\dot{N}$	Molar flow	$[\mathrm{mol\,s^{-1}}]$
N	Number of trays of a distillation column	[–]
n	Amount of moles	[mol]
n/iso	Ratio of linear and branched aldehydes	$[\mathrm{mol\,mol^{-1}}]$
p	Pressure	[bar abs]
q	Controls	[various]
$\tilde{R}$	Universal gas constant	$[\mathrm{J\,mol^{-1}\,K^{-1}}]$
r	Reaction rate	$[\mathrm{mol/g_{cat}/min}]$
$\tilde{r}$	Reaction rate	$[\mathrm{mol\,L^{-1}\,min^{-1}}]$
S	Selectivity	$[\mathrm{mol\,mol^{-1}}]$
T	Temperature	[K]
t	Time	[s]
t_B	Batch time	[s]
t_D	Time of the continuous (downstream) process	[s]
t_I	Preparation time	[s]
u	Controls	[various]
V	Volume	[mL]
$\dot{V}$	Volumetric flow rate	$[\mathrm{mL\,min^{-1}}]$
w	Mass fraction	$[\mathrm{g\,g^{-1}}]$
X	Conversion	$[\mathrm{mol\,mol^{-1}}]$

x	Molar fraction	$[\mathrm{mol\,mol^{-1}}]$
$\hat{x}$	Input states of the Kriging model	$[\mathrm{mol\,mol^{-1}}]$
y	Gas phase molar fraction	$[\mathrm{mol\,mol^{-1}}]$

Subscripts & Superscripts

0	Initial condition / condition at $t = 0$
α	Running index for species
AP	Apolar
β	Running index for species
Bott	Bottom
B	Batch
Dist	Distillate stream
cat	Catalyst
cycle	Process cycle
D	Continuous stage
DBuffer	Flash buffer tank
Dec	Decanter
DistCol	Distillation column
Feed	Feed

fresh	Fresh components entering the process
gas	Gaseous phase
HK	High key component
idle	Simulation stage without reaction
in	Inlet
init	Initial
I	Idle stage
i	Running index
j	Running index
Kaiser	Reference to Kaiser et al. [1]
k	Running index
L	Liquid
liq	Liquid phase
LK	Light key component
m	Running index
$make-up$	Make-up
max	Maximal
mean	Mean value
min	Minimal
n	Running index

opt Optimal

out Outlet

P Polar

ref Reference value

sat Saturate

target Target / Set-point value

tot Total

UBuffer Feed buffer tank

References

[1] N. M. Kaiser, M. Jokiel, K. McBride, R. J. Flassig, K. Sundmacher, Optimal Reactor Design via Flux Profile Analysis for an Integrated Hydroformylation Process, Industrial & Engineering Chemistry Research 56 (2017) 11507–11518. URL: http://pubs.acs.org/doi/10.1021/acs.iecr.7b01939. doi:10.1021/acs.iecr.7b01939.

[2] H. Freund, K. Sundmacher, Towards a methodology for the systematic analysis and design of efficient chemical processes, Chemical Engineering and Processing: Process Intensification 47 (2008) 2051–2060. URL: http://linkinghub.elsevier.com/retrieve/pii/S0255270108001669. doi:10.1016/j.cep.2008.07.011.

[3] N. M. Kaiser, R. J. Flassig, K. Sundmacher, Reactor-network synthesis via flux profile analysis, Chemical Engineering Journal 335 (2018) 1018–1030. URL: http://linkinghub.elsevier.com/retrieve/pii/S1385894717315474. doi:10.1016/j.cej.2017.09.051.

[4] A. Behr, C. Fängewisch, Temperature-Dependent Multicomponent Solvent Systems – An Alternative Concept for Recycling Homogeneous Catalysts, Chemical Engineering & Technology 25 (2002) 143–147. URL: http://onlinelibrary.wiley.com/doi/10.1002/1521-4125(200202)25:2<143::AID-CEAT143>3.0.CO;2-O/abstract. doi:10.1002/1521-4125(200202)25:2<143::AID-CEAT143>3.0.CO;2-O.

[5] J. M. Dreimann, H. Warmeling, J. N. Weimann, K. Künnemann, A. Behr, A. J. Vorholt, Increasing selectivity of the hydroformylation in a miniplant: Catalyst, solvent, and olefin recycle in two loops, AIChE Journal 62 (2016) 4377–4383. doi:10.1002/aic.15345.

[6] A. Behr, A. J. Vorholt, Homogeneous Catalysis with Renewables, volume 39 of *Catalysis by Metal Complexes*, Springer International Publishing, Cham, 2017. URL: http://link.springer.com/10.1007/978-3-319-54161-7. doi:10.1007/978-3-319-54161-7.

[7] B. Hentschel, A. Peschel, H. Freund, K. Sundmacher, Simultaneous design of the optimal reaction and process concept for multiphase systems, Chemical Engineering Science 115 (2014) 69–87. URL: http://linkinghub.elsevier.com/retrieve/pii/S0009250913006659. doi:10.1016/j.ces.2013.09.046.

[8] C. W. Kohlpaintner, R. W. Fischer, B. Cornils, Aqueous biphasic catalysis: Ruhrchemie/Rhône-Poulenc oxo process, Applied Catalysis A: General 221 (2001) 219–225.

[9] P. W. Van Leeuwen, C. Claver, Rhodium catalyzed hydroformylation, volume 22, Springer Science & Business Media, 2002.

[10] H.-J. Arpe, K. Weissermel, Industrial organic chemistry, fifth, completely revised edition ed., Wiley-VCH, Weinheim, Germany, 2010.

[11] O. Walter, Multiphase homogeneous catalysis. edited by b. cornils, w. a. herrmann, i. t. horváth, w. leitner, s. mecking, h. olivier-bourbigou and d. vogt., Angewandte Chemie International Edition 45 (2006) 2005–2005. URL: http://dx.doi.org/10.1002/anie.200585366. doi:10.1002/anie.200585366.

[12] F. Van Vyve, A. Renken, Hydroformylation in reverse micellar systems, Catalysis Today 48 (1999) 237 – 243. URL: http://www.sciencedirect.com/science/article/pii/S0920586198003782. doi:https://doi.org/10.1016/S0920-5861(98)00378-2.

[13] M. Li, Y. Li, H. Chen, Y.-e. He, X. Li, Studies on 1-dodecene hydroformylation in biphasic catalytic system containing mixed micelle, Journal of Molecular Catalysis A: Chemical 194 (2003) 13 – 17. URL: http://www.sciencedirect.com/science/article/pii/S1381116902005332. doi:https://doi.org/10.1016/S1381-1169(02)00533-2.

[14] A. Riisager, R. Fehrmann, M. Haumann, P. Wasserscheid, Supported Ionic Liquid Phase (SILP) Catalysis: An Innovative Concept for Homogeneous Catalysis in Continuous Fixed-Bed Reactors, European Journal of Inorganic Chemistry 2006 (2006) 695–706. URL: http://doi.wiley.com/10.1002/ejic.200500872. doi:10.1002/ejic.200500872.

[15] H. Jin, B. Subramaniam, A. Ghosh, J. Tunge, Intensification of catalytic olefin hydroformylation in CO2-expanded media, AIChE Journal 52 (2006) 2575–2581. URL: http://doi.wiley.com/10.1002/aic.10882. doi:10.1002/aic.10882.

[16] S. Bektesevic, A. M. Kleman, A. E. Marteel-Parrish, M. A. Abraham, Hydroformylation in supercritical carbon dioxide: Catalysis and benign solvents, The Journal of Supercritical Fluids 38 (2006) 232–241. URL:

http://linkinghub.elsevier.com/retrieve/pii/S0896844606001057. doi:10.1016/j.supflu.2006.01.019.

[17] A. Behr, G. Henze, L. Johnen, C. Awungacha, Advances in thermomorphic liquid/liquid recycling of homogeneous transition metal catalysts, Journal of Molecular Catalysis A: Chemical 285 (2008) 20–28. doi:10.1016/j.molcata.2008.01.021.

[18] E. Schäfer, Y. Brunsch, G. Sadowski, A. Behr, Hydroformylation of 1-Dodecene in the Thermomorphic Solvent System Dimethylformamide/Decane. Phase Behavior–Reaction Performance–Catalyst Recycling, Industrial & Engineering Chemistry Research 51 (2012) 10296–10306. URL: http://pubs.acs.org/doi/10.1021/ie300484q. doi:10.1021/ie300484q.

[19] G. Kiedorf, D. Hoang, A. Müller, A. Jörke, J. Markert, H. Arellano-Garcia, A. Seidel-Morgenstern, C. Hamel, Kinetics of 1-dodecene hydroformylation in a thermomorphic solvent system using a rhodium-biphephos catalyst, Chemical Engineering Science 115 (2014) 31–48. URL: http://linkinghub.elsevier.com/retrieve/pii/S000925091300434X. doi:10.1016/j.ces.2013.06.027.

[20] B. Hentschel, G. Kiedorf, M. Gerlach, C. Hamel, A. Seidel-Morgenstern, H. Freund, K. Sundmacher, Model-Based Identification and Experimental Validation of the Optimal Reaction Route for the Hydroformylation of 1-Dodecene, Industrial & Engineering Chemistry Research 54 (2015) 1755–1765. URL: http://pubs.acs.org/doi/10.1021/ie504388t. doi:10.1021/ie504388t.

[21] J. Dreimann, P. Lutze, M. Zagajewski, A. Behr, A. Górak, A. J. Vorholt, Highly integrated reactor–separator systems for the recycling of homogeneous catalysts, Chemical Engineering and Processing: Process Intensification 99 (2016) 124–131. doi:10.1016/j.cep.2015.07.019.

[22] B. Hentschel, G. Kiedorf, M. Gerlach, C. Hamel, A. Seidel-Morgenstern, H. Freund, K. Sundmacher, Model-Based Identification and Experimental Validation of the Optimal Reaction Route for the Hydroformylation of 1-Dodecene, Industrial & Engineering Chemistry Research 54 (2015) 1755–1765. doi:10.1021/ie504388t.

[23] B. Hentschel, A. Peschel, M. Xie, C. Vogelpohl, G. Sadowski, H. Freund, K. Sundmacher, Model-based prediction of optimal conditions for 1-octene hydroformylation, Chemical Engineering Science 115 (2014) 58–68. URL: http://linkinghub.elsevier.com/retrieve/pii/S0009250913002352. doi:10.1016/j.ces.2013.03.051.

[24] K. McBride, N. M. Kaiser, K. Sundmacher, Integrated reaction–extraction process for the hydroformylation of long-chain alkenes with a homogeneous catalyst, Computers & Chemical Engineering 105 (2017) 212–223. doi:10.1016/j.compchemeng.2016.11.019.

[25] N. M. Kaiser, R. J. Flassig, K. Sundmacher, Probabilistic reactor design in the framework of elementary process functions, Computers & Chemical Engineering 94 (2016) 45–59. URL: http://linkinghub.elsevier.com/retrieve/pii/S0098135416301983. doi:10.1016/j.compchemeng.2016.06.008.

[26] K. McBride, T. Gaide, A. Vorholt, A. Behr, K. Sundmacher, Thermomorphic solvent selection for homogeneous catalyst recovery based on COSMO-RS, Chemical Engineering and Processing: Process Intensification 99 (2016) 97–106. URL: http://linkinghub.elsevier.com/retrieve/pii/S0255270115300568. doi:10.1016/j.cep.2015.07.004.

[27] E. Schäfer, Y. Brunsch, G. Sadowski, A. Behr, Hydroformylation of 1-Dodecene in the Thermomorphic Solvent System Dimethylformamide/Decane. Phase Behavior–Reaction Performance–Catalyst Recycling, Industrial & Engineering Chemistry Research 51 (2012) 10296–10306. doi:10.1021/ie300484q.

[28] P. W. Van Leeuwen, C. Claver, Rhodium catalyzed hydroformylation, volume 22, Springer Science & Business Media, 2002.

[29] A. J. V. D. Schaft, J. M. Schumacher, Complementarity Modeling of Hybrid Systems, 1998.

[30] B. Baumrucker, L. Biegler, MPEC strategies for optimization of a class of hybrid dynamic systems, Journal of Process Control 19 (2009) 1248–1256. URL: http://linkinghub.elsevier.com/retrieve/pii/S0959152409000365. doi:10.1016/j.jprocont.2009.02.006.

[31] M. P. Avraam, N. Shah, C. C. Pantelides, Modelling and Optimisation of General Hybrid Systems in the Continuous Time Domain, Computers & Chemical Engineering 22 (1998) 221–228.

[32] J. Oldenburg, W. Marquardt, Disjunctive modeling for optimal control of hybrid systems, Computers & Chemical Engineering 32 (2008) 2346–2364. URL: http://linkinghub.elsevier.com/retrieve/pii/S0098135407002931. doi:10.1016/j.compchemeng.2007.12.002.

[33] B. Baumrucker, J. Renfro, L. Biegler, MPEC problem formulations and solution strategies with chemical engineering applications, Computers & Chemical Engineering 32 (2008) 2903–2913. URL: http://linkinghub.elsevier.com/retrieve/pii/S0098135408000367. doi:10.1016/j.compchemeng.2008.02.010.

[34] J. Andersson, A General-Purpose Software Framework for Dynamic Optimization, PhD thesis, Arenberg Doctoral School, KU Leuven, Department of Electrical Engineering (ESAT/SCD) and Optimization in Engineering Center, Kasteelpark Arenberg 10, 3001-Heverlee, Belgium, 2013.

[35] G. van Rossum, et al., The Python Language Reference, 2018. URL: http://docs.python.org/release/3.6.6/reference/index.html.

[36] A. Wächter, L. T. Biegler, On the implementation of an interior-point filter line-search algorithm for large-scale nonlinear programming, Mathematical programming 106 (2006) 25–57.

[37] HSL, A collection of Fortran codes for large scale scientific computation., http://www.hsl.rl.ac.uk/, n.a.

Supplementary Materials

Cyclic Operation of a Semi-Batch Reactor for the Hydroformylation of Long-Chain Olefins and Integration in a Continuous Production Process

Karsten H. G. Rätze[a], Michael Jokiel[b], Nicolas M. Kaiser[a], and Kai Sundmacher[a,b,*]

[a] *Otto von Guericke University Magdeburg, Chair for Process Systems Engineering, Universitätsplatz 2, D-39106 Magdeburg, Germany*

[b] *Max Planck Institute for Dynamics of Complex Technical Systems, Department Process Systems Engineering, Sandtorstr. 1, D-39106 Magdeburg, Germany*

[*] *sundmacher@mpi-magdeburg.mpg.de*

A. Model Equations

The process models consist of individual units which are combined in an overall process model. In the following, the process unit equations as well as additional equations comprising the reaction rate equations are summarized.

A.1. Reaction Rate Equations

The hydroformylation is performed as a homogeneously catalyzed reaction in a TMS-system consisting of the solvent pair n-decane/DMF. As catalyst, $Rh(acac)(CO)_2$ is used as a precursor with BiPhePhos as the ligand. Hentschel et al. [20] published refined reaction rate equations with an underlying reaction network involving six reaction paths (see Figure 1). These reaction rate equations are also used in this work and summarized below

$$r_1 = \frac{k_1\left(T\right) c_{\mathrm{1C12en}} c_{\mathrm{H_2}} c_{\mathrm{CO}}}{1 + K_{1,1} c_{\mathrm{1C12en}} + K_{1,2} c_{\mathrm{nC13al}} + K_{1,3} c_{\mathrm{H_2}}}, \tag{A.1}$$

$$r_2 = \frac{k_2\left(T\right) \left(c_{\mathrm{1C12en}} - \frac{c_{\mathrm{iC12en}}}{K_{\mathrm{p},2}}\right)}{1 + K_{2,1} c_{\mathrm{1C12en}} + K_{2,2} c_{\mathrm{iC12en}}}, \tag{A.2}$$

$$r_3 = \frac{k_3\left(T\right) \left(c_{\mathrm{1C12en}} c_{\mathrm{H_2}} - \frac{c_{\mathrm{nC12an}}}{K_{\mathrm{p},3}}\right)}{1 + K_{3,1} c_{\mathrm{1C12en}} + K_{3,2} c_{\mathrm{nC12an}} + K_{3,3} c_{\mathrm{H_2}}}, \tag{A.3}$$

$$r_4 = k_4\left(T\right) c_{\mathrm{iC12en}} c_{\mathrm{H_2}}, \tag{A.4}$$

$$r_5 = k_5\left(T\right) c_{\mathrm{iC12en}} c_{\mathrm{H_2}} c_{\mathrm{CO}}, \tag{A.5}$$

$$r_6 = k_6\left(T\right) c_{\mathrm{1C12en}} c_{\mathrm{H_2}} c_{\mathrm{CO}}. \tag{A.6}$$

Because of the reaction rates being calculated based on the catalyst metal mass, reaction rates based on the liquid volume can be achieved using

$$\tilde{r}_j = c_{\mathrm{cat}} \tilde{M}_{\mathrm{cat}} r_j, \tag{A.7}$$

with $\tilde{M}_{\mathrm{cat}} = 258.03\,\mathrm{g\,mol^{-1}}$ [19]. The concentration of active catalyst is determined by an equilibrium and can be calculated using

$$c_{\mathrm{cat}} = \frac{c_{\mathrm{cat,tot}}}{1 + K_{\mathrm{cat},1} c_{\mathrm{CO}}^{K_{\mathrm{cat},3}} + K_{\mathrm{cat},2} \frac{c_{\mathrm{CO}}^{K_{\mathrm{cat},3}}}{c_{\mathrm{H_2}}}}, \tag{A.8}$$

where $c_{\mathrm{cat,tot}}$ represents the total catalyst concentration in the process unit and c_{cat} the concentration of active catalyst. The temperature dependent reaction rate coefficients k_j are calculated using an Arrhenius approach with $T_{\mathrm{ref}} = 378.15\,\mathrm{K}$ [20]

$$k_j = k_{j,0} \exp\left(\frac{-E_{\mathrm{A},j}}{\tilde{R}} \left(\frac{1}{T} - \frac{1}{T_{\mathrm{ref}}}\right)\right), \qquad j \in \mathrm{RCT} \tag{A.9}$$

and the equilibrium constants result from

$$K_{\mathrm{p},j} = \exp\left(\frac{-\Delta G_j}{\tilde{R}T}\right), \tag{A.10}$$

$$\Delta G_j = a_{0,j} + a_{1,j} T + a_{2,j} T^2 \qquad j \in 2, 3. \tag{A.11}$$

Parameters for the reaction rate equations are taken from Kaiser et al. [1] and can be found in Tables A.1 and A.2.

A.2. Reactor Indices

The reactor performance is measured using the conversion, selectivity and the ratio of linear to branched aldehyde (n/iso). Concentrations are used to ensure consistency between the steady-state and dynamic model since the conservation of mass is violated for the steady-state model by averaging the outlet flow of the flash buffer tank in Eq. (4). The performance measures are defined as follows

$$X_{\mathrm{1C12en}} = 1 - \frac{c_{\mathrm{1C12en,in}}^{\mathrm{Dec}}}{c_{\mathrm{1C12en}}^{\mathrm{SBR}}(t=0)} \tag{A.12}$$

$$S_{\mathrm{nC13al}} = \frac{c_{\mathrm{nC13al,in}}^{\mathrm{Dec}} - c_{\mathrm{nC13al}}^{\mathrm{SBR}}(t=0)}{c_{\mathrm{1C12en}}^{\mathrm{SBR}}(t=0) - c_{\mathrm{1C12en,in}}^{\mathrm{Dec}}} \tag{A.13}$$

$$n/iso = \frac{c_{\mathrm{nC13al,in}}^{\mathrm{Dec}}}{\left(c_{\mathrm{nC13al,in}} + c_{\mathrm{iC13al,in}}\right)^{\mathrm{Dec}}}. \tag{A.14}$$

Table A.1: Parameters for the reaction rate equations

j	$E_{\mathrm{A},j}$			$k_{j,0}$	$K_{j,1}$	$K_{j,2}$	$K_{j,3}$
	[kJ mol^{-1}]			[.]	[mL mol^{-1}]	[mL/mol]	[mL mol^{-1}]
1	113.08	4.904	$\times 10^{16}$	mL^3 g^{-1} min^{-1} mol^{-2}	574 876.0	3 020 413.0	11 732 838.0
2	136.89	4.878	$\times 10^{6}$	mL g^{-1} min^{-1}	38 632.0	223 214.0	0.0
3	76.11	2.724	$\times 10^{8}$	mL^2 g^{-1} min^{-1} mol^{-1}	2661.2	7100.0	1280.0
4	102.26	2.958	$\times 10^{4}$	mL^2 g^{-1} min^{-1} mol^{-1}	0.0	0.0	0.0
5	120.84	3.702	$\times 10^{10}$	mL^3 g^{-1} min^{-1} mol^{-2}	0.0	0.0	0.0
6	113.08	3.951	$\times 10^{11}$	mL^3 g^{-1} min^{-1} mol^{-2}	0.0	0.0	0.0
cat	-		-	–	30 410	0.0	0.644

Table A.2: Gibbs Energy parameters

		ΔG_2	ΔG_3
	[.]		
a_0	J mol^{-1}	$-1.100\,34 \times 10^4$	$-1.262\,750 \times 10^5$
a_1	J mol^{-1} K^{-1}	0.0	1.266×10^2
a_2	J mol^{-1} K^{-2}	0.0	6.803×10^{-3}

A.3. Repeated Semi-Batch Reactor (RSBR)

The repeated semi-batch reactor is described using molar balances of the liquid phase as well as gaseous phase. For the liquid phase,

$$\frac{\mathrm{d}n_\alpha^{\mathrm{liq}}}{\mathrm{d}t} = V_\mathrm{L} \sum_j \nu_{\alpha,j} \tilde{r}_j \quad \forall \alpha \in \mathrm{SPC}, \tag{A.15}$$

$$\frac{\mathrm{d}n_\alpha^{\mathrm{liq}}}{\mathrm{d}t} = V_\mathrm{L} \left[k_\mathrm{L} a \cdot \left(c_\alpha^{\mathrm{sat}} - c_\alpha \right) + \sum_j \nu_{\alpha,j} \tilde{r}_j \right] \quad \forall \alpha \in \mathrm{GAS}, \tag{A.16}$$

summarize the influence of the reactions as well as the gas-liquid transport of the permanent gases CO and H_2 into the reaction mixture. The gas phase is described using

$$\frac{\mathrm{d}n_\alpha^{\mathrm{gas}}}{\mathrm{d}t} = j_\alpha - V_\mathrm{L} k_\mathrm{L} a \cdot \left(c_\alpha^{\mathrm{sat}} - c_\alpha \right) \quad \forall \alpha \in \mathrm{GAS}, \tag{A.17}$$

and the ideal gas assumption to calculate the corresponding partial pressures and gas phase compositions. The liquid phase in the semi-batch reactor is assumed to be ideally mixed and the liquid volume as well as the density of the liquid phase are determined using

$$V_\mathrm{L}(n,T) = \frac{\sum_{\alpha \in \mathrm{SPC}} \tilde{M}_\alpha \cdot n_\alpha}{\rho(n,T)}, \tag{A.18}$$

$$\rho(n,T) = \left(\sum_{\alpha \in \mathrm{SPC}} \frac{\frac{\tilde{M}_\alpha \cdot n_\alpha}{\sum_{\beta \in \mathrm{SPC}} \tilde{M}_\beta \cdot n_\beta}}{\rho_\alpha} \right)^{-1}, \tag{A.19}$$

$$\rho_\alpha(T) = a_{\rho,0,\alpha} + a_{\rho,1,\alpha} \cdot T \quad \forall \alpha \in \mathrm{SPC}. \tag{A.20}$$

The parameters for calculating the density can be found in Table A.3.

A.4. Flash Buffer Tank (DBuffer)

The flash buffer tank is located after the SBR and its behavior is described with separate models for the steady-state and the dynamic process model. In the case of the steady-state model, the liquid phase of the flash buffer tank is governed by the following set of ODEs

Table A.3: Density parameters and molar masses taken from McBride et al. [24].

α	$a_{\rho,0,\alpha}$ [kg m^{-3}]	$a_{\rho,1,\alpha}$ [kg m^{-3} K^{-1}]	$\tilde{M}_\alpha$ [g mol^{-1}]
C10an	981.5951	−0.835 36	142.2817
DMF	1256.5163	−1.0306	73.0938
1C12en	993.8919	−0.788 75	168.3190
iC12en	993.8919	−0.788 75	168.3190
nC13al	1068.1228	−0.801 80	198.3449
iC13al	1068.1228	−0.801 80	198.3449
nC12an	977.0381	−0.767 43	170.3348
H_2	–	–	2.0159
CO	–	–	28.0101

$$\frac{\mathrm{d}c_\alpha}{\mathrm{d}t} = \sum_{j \in \mathrm{RCT}} \nu_{\alpha,j} \tilde{r}_j \quad \forall \alpha \in \mathrm{SPC}, \tag{A.21}$$

$$\frac{\mathrm{d}c_\alpha}{\mathrm{d}t} = k_\mathrm{L} a \cdot \left(c_\alpha^\mathrm{sat} - c_\alpha\right) + \sum_{j \in \mathrm{RCT}} \nu_{\alpha,j} \tilde{r}_j \quad \forall \alpha \in \mathrm{GAS}, \tag{A.22}$$

$$\frac{\mathrm{d}c_\mathrm{cat}}{\mathrm{d}t} = 0. \tag{A.23}$$

In order to determine the volumetric flow from the flash buffer tank to the subsequent process unit, the liquid hold-up of the SBR is employed leading to

$$\dot{V}_\mathrm{out} = \frac{\varepsilon_\mathrm{L}^\mathrm{SBR} V^\mathrm{SBR}}{t_\mathrm{D}}, \tag{A.24}$$

with the liquid hold-up ε_L, the total vessel volume V and the time of one process cycle t_D.

In contrast to that, the flash buffer tank model for the dynamic process model contains the molar balances for the liquid phase

$$\frac{\mathrm{d}n_\alpha}{\mathrm{d}t} = -\dot{V}_{\mathrm{out}} c_\alpha + V_{\mathrm{L}} \sum_{j \in \mathrm{RCT}} \nu_{\alpha,j} \tilde{r}_j \quad \forall \alpha \in \mathrm{SPC}, \tag{A.25}$$

$$\frac{\mathrm{d}n_\alpha}{\mathrm{d}t} = -\dot{V}_{\mathrm{out}} c_\alpha + V_{\mathrm{L}} \left[k_{\mathrm{L}} a \cdot \left(c_\alpha^{\mathrm{sat}} - c_\alpha \right) + \sum_{j \in \mathrm{RCT}} \nu_{\alpha,j} \tilde{r}_j \right] \quad \forall \alpha \in \mathrm{GAS}, \tag{A.26}$$

$$\frac{\mathrm{d}n_{\mathrm{cat}}}{\mathrm{d}t} = -\dot{V}_{\mathrm{out}} c_{\mathrm{cat}}, \tag{A.27}$$

resulting in an accurate depiction of the shrinking liquid hold-up in the buffer tank over one process cycle. Similar to the SBR, the liquid phase of the process unit is assumed to be ideally mixed. The volumetric flow is used as a control variable to determine the maximal allowed flow rate considering restrictions on the composition in the feed buffer tank. By describing the change of liquid hold-up over time, it is also possible to approximate the change of pressure without employing rigorous balances for the gaseous phase by assuming ideal gas behavior and isothermal conditions in the buffer tank. This leads to the additional algebraic equation

$$p(t) = p_0 \cdot \frac{1 - \frac{V_{\mathrm{L},0}}{V}}{1 - \frac{V_{\mathrm{L}}(t)}{V}}, \tag{A.28}$$

where p_0 and $V_{\mathrm{L},0}$ are the pressure and liquid volume at the beginning of each cycle, respectively. Whereas $V_{\mathrm{L},0}$ is taken from the simulation results of the SBR, experimental data is used for p_0.

A.5. Continuously Stirred Tank Reactor (CSTR)

For the CSTR, a steady-state model is used governed by the algebraic equations

$$\dot{N}_{\alpha,\mathrm{out}} = \dot{N}_{\alpha,\mathrm{in}} + V_{\mathrm{L}} \sum_{j \in \mathrm{RCT}} \nu_{\alpha,j} \tilde{r}_j \quad \forall \alpha \in \mathrm{SPC}, \tag{A.29}$$

$$\dot{N}_{\alpha,\mathrm{out}} = \dot{N}_{\alpha,\mathrm{in}} + V_{\mathrm{L}} \left[k_{\mathrm{L}} a \cdot \left(c_\alpha^{\mathrm{sat}} - c_\alpha \right) + \sum_{j \in \mathrm{RCT}} \nu_{\alpha,j} \tilde{r}_j \right] \quad \forall \alpha \in \mathrm{GAS}, \tag{A.30}$$

for the liquid phase. The gaseous phase is not modeled in detail but described using the pressure p and the gas phase composition y.

A.6. Decanter (Dec)

The liquid-liquid phase separation of the considered TMS-system was investigated by McBride et al. [24]. By using a Kriging Model as surrogate model, they were able to accurately predict the partition coefficients for the different species in the reaction mixture. By grouping similar species, only four input variables $k \in \{\mathrm{DMF}, \mathrm{C10an} + \mathrm{nC12an}, \mathrm{nC13al} + \mathrm{iC13al}, \mathrm{1C12en} + \mathrm{iC12en}, T\}$ need to be considered, so that the partition coefficients for the polar phase can be calculated for $m \in \{\mathrm{DMF}, \mathrm{C10an}, \mathrm{nC13al}, \mathrm{1C12en}, \mathrm{BiPhePhos}\}$ using

$$\theta_m^{\mathrm{P}} = \mathrm{KR}\left(\hat{x}_k, T\right). \tag{A.31}$$

By utilizing

$$\theta_m^{\mathrm{P}} = \frac{n_m^{\mathrm{P}}}{n_m^{\mathrm{P}} + n_m^{\mathrm{AP}}} = \frac{\dot{N}_m^{\mathrm{P}}}{\dot{N}_m^{\mathrm{P}} + \dot{N}_m^{\mathrm{AP}}}, \tag{A.32}$$

the molar amount in the polar and apolar phase can be calculated.

A.7. Distillation Column (DistCol)

The number of trays as well as the distillate and bottom stream of the distillation column are described using the Fenske-Underwood correlations

$$N_{\min} = \frac{\ln \frac{(x_{\mathrm{LK}}/x_{\mathrm{HK}})_{\mathrm{Dist}}}{(x_{\mathrm{LK}}/x_{\mathrm{HK}})_{\mathrm{Bott}}}}{\ln \alpha_{\mathrm{LK,HK}}} = \frac{\ln \frac{\dot{N}_{\mathrm{LK}}^{\mathrm{Dist}} \cdot \dot{N}_{\mathrm{HK}}^{\mathrm{Bott}}}{\dot{N}_{\mathrm{LK}}^{\mathrm{Bott}} \cdot \dot{N}_{\mathrm{HK}}^{\mathrm{Dist}}}}{\ln \alpha_{\mathrm{LK,HK}}}, \tag{A.33}$$

$$\alpha_{i,j} \approx \frac{p_i^{\mathrm{sat}}}{p_j^{\mathrm{sat}}}, \tag{A.34}$$

$$p_i^{\mathrm{sat}} = 10^{\left(a_0 + \frac{a_1}{T} + a_2 \log_{10} T + a_3 T + a_4 T^2\right)} \cdot 133.322 \cdot 10^{-6} \quad \forall i \in \mathrm{SPC} \setminus \{\mathrm{iC12en}, \mathrm{iC13al}\}, \tag{A.35}$$

$$p_i^{\mathrm{sat}} = 0.1 \cdot \exp\left(a_0 + \frac{a_1}{T} + a_2 \ln T + a_3 T^{a_4}\right) \quad \forall i \in \{\mathrm{iC12en}, \mathrm{iC13al}\}. \tag{A.36}$$

The parameters for calculating p_i^{sat} are taken from McBride et al. [24] and summarized in Table A.4.

As light key (LK) and heavy key (HK) components, iC12en and nC13al are chosen, respectively. In order to account for changes in the relative volatility over the column height, the calculation is

Table A.4: Vapour pressure parameters

	a_0	a_1	a_2	a_3	a_4
C10an	26.5125	−3358.4	−6.1174	-3.3225×10^{-10}	4.8554×10^{-7}
DMF	−47.9857	−2385.0	28.8000	-5.8596×10^{-2}	3.1386×10^{-5}
1C12en	−8.5899	−3524.1	10.8060	-2.8161×10^{-2}	1.4267×10^{-5}
iC12en	75.7900	−9964.0	−8.9650	4.94×10^{-18}	6
nC13al	161.5042	−9766.0	−55.5910	2.1036×10^{-2}	5.5498×10^{-13}
iC13al	10.4200	−6149.0	0.1970	-2×10^{-4}	1
nC12an	−5.5630	−3470.0	9.0270	-2.319×10^{-2}	1.124×10^{-5}

performed for n different trays (normally at the top and bottom of the distillation column) and averaged using the geometric average

$$\overline{\alpha}_{\mathrm{LK,HK}} = \sqrt[n]{\prod_n \alpha_{\mathrm{LK,HK}}{}^{(n)}}. \tag{A.37}$$

By using Eq. (A.37) in Eq. (A.33) and specifying the recovery ζ^{Dist} of the light and heavy key components in the distillate stream, $\dot{N}_{\mathrm{LK}}^{\mathrm{Dist}}$ and $\dot{N}_{\mathrm{LK}}^{\mathrm{Bott}}$ as well as $\dot{N}_{\mathrm{HK}}^{\mathrm{Dist}}$ and $\dot{N}_{\mathrm{HK}}^{\mathrm{Bott}}$ can be calculated via

$$\dot{N}_k^{\mathrm{Dist}} = \zeta_k^{\mathrm{Dist}} \dot{N}_{\mathrm{in}}, \tag{A.38}$$

$$\dot{N}_k^{\mathrm{Bott}} = \left(1 - \zeta_k^{\mathrm{Dist}}\right) \dot{N}_{\mathrm{in}} \quad \forall k \in \{\mathrm{LK}, \mathrm{HK}\}, \tag{A.39}$$

leading to the minimal number of trays N_{min}. Based on these information, all of the other component's bottom and distillate molar flow rates can be calculated using

$$\dot{N}_{\alpha}^{\mathrm{Bott}} = \frac{\dot{N}_{\alpha}^{\mathrm{Feed}}}{1 + \frac{\dot{N}_{\mathrm{HK}}^{\mathrm{Dist}}}{\dot{N}_{\mathrm{HK}}^{\mathrm{Bott}}} \overline{\alpha}_{i,\mathrm{HK}}^{N_{\mathrm{min}}}}, \tag{A.40}$$

$$\dot{N}_{\alpha}^{\mathrm{Dist}} = \dot{N}_{\alpha}^{\mathrm{Feed}} - \dot{N}_{\alpha}^{\mathrm{Bott}} \quad \forall \alpha \in \mathrm{SPC}. \tag{A.41}$$

A.8. Feed Buffer Tank (UBuffer)

The liquid phase of the feed buffer tank preceding the SBR can be described with the following set of ODEs

$$\frac{\mathrm{d}n_{\alpha}}{\mathrm{d}t} = \sum_{k \in \mathrm{UBufferInput}} \dot{N}_{\alpha,k} \quad \forall \alpha \in \mathrm{SPC}, \tag{A.42}$$

$$\frac{\mathrm{d}n_{\alpha}}{\mathrm{d}t} = V_{\mathrm{L}} k_{\mathrm{L}} a \cdot \left(c_{\alpha}^{\mathrm{sat}} - c_{\alpha}\right) \quad \forall \alpha \in \mathrm{GAS}, \tag{A.43}$$

$$\frac{\mathrm{d}n_{\mathrm{cat}}}{\mathrm{d}t} = \sum_{k \in \mathrm{UBufferInput}} \dot{N}_{\mathrm{cat},k}. \tag{A.44}$$

As in the case of the flash buffer tank, the model for the feed buffer tank assumes ideal mixing of the liquid phase and accounts for the change in pressure inside of the vessel by assuming ideal gas behavior and isothermal conditions. The relation of the pressure and liquid volume can be found in Eq. (A.28) with p_0 being determined experimentally and $V_{\mathrm{L},0}$ being set to zero at the beginning of each new cycle.

B. Optimization Problem Formulation

The hydroformylation process is analyzed using a steady-state and a dynamic process model with different process configurations. In the following, the optimization problems for each of the analyzed cases is introduced alongside their corresponding model parameters.

B.1. Steady-State

In the case study denoted as *Reference*, the steady-state model is compared to the results from Kaiser et al. [1]. DOP1

$$\min_{u(t),q} \quad -S_{\mathrm{nC13al}} \tag{DOP1}$$

s.t.

reaction rates	Eq. $(A.1 - A.11)$,
gas solubility	Eq. $(2 - 3)$,
constitutive equations	Eq. $(A.18 - A.20)$,
component mass balances	Eq. $(A.15 - A.17)$,
	Eq. $(A.21 - A.24)$,
	Eq. $(A.29 - A.30)$,
	Eq. $(A.33 - A.41)$,
phase separation	Eq. $(A.31 - A.32)$,
flowsheet	Eq. $(4 - 9)$,
residence time	Eq. $(1, 10 - 12)$,
reactor indices	Eq. $(A.12 - A.14)$,
	Eq. $(B.1)$,
	$n/iso \geq 0.95$,
initial conditions, LB, UB	Table $B.1$ and $B.2$,
temperature	$0 = T^{\mathrm{DBuffer}}(t) - T^{\mathrm{SBR}}(t_{\mathrm{B}})$,
pressure	$0 = p^{\mathrm{DBuffer}}(t) - p^{\mathrm{SBR}}(t_{\mathrm{B}})$,
gas phase composition	$\sum_{\alpha \in \mathrm{GAS}} y_{\alpha}^{\mathrm{SBR}}(t) = 1, \sum_{\alpha \in \mathrm{GAS}} y_{\alpha}^{\mathrm{CSTR}} = 1,$
	$0 = y_{\alpha}^{\mathrm{DBuffer}}(t) - y_{\alpha}^{\mathrm{SBR}}(t_{\mathrm{B}}) \quad \forall \alpha \in \mathrm{GAS},$
stream constraints	$\dot{N}_{\alpha}(t) \geq 0 \quad \forall \alpha \in \mathrm{SPC} \cup \mathrm{GAS},$
composition constraints	$c_{\alpha}(t) \geq 0,\, n_{\alpha}(t) \geq 0 \quad \forall \alpha \in \mathrm{SPC} \cup \mathrm{GAS},$
controls	$u(t) = \left[T^{\mathrm{SBR}}(t), j_{\mathrm{CO}}^{\mathrm{SBR}}(t), j_{\mathrm{H_2}}^{\mathrm{SBR}}(t)\right],$
	$q = \left[T^{\mathrm{CSTR}}, p^{\mathrm{CSTR}}, y_{\mathrm{CO}}^{\mathrm{CSTR}}, y_{\mathrm{H_2}}^{\mathrm{CSTR}}, \xi^{\mathrm{Dec}}, \xi^{\mathrm{DistCol}}\right],$

summarizes the optimization problem used in an optimization study performed for different conversion levels. Initialization of the problem is done using

$$m_{\mathrm{1C12en,init}}^{\mathrm{SBR}} = 40\,\mathrm{g}, \qquad \dot{N}_{\mathrm{make-up,init}} = \vec{0}, \qquad n_{\mathrm{init}}^{\mathrm{SBR,gas}} = \frac{y_{\mathrm{init}} p_{\mathrm{init}} V^{\mathrm{gas}}}{\tilde{R}T},$$

as well as Table B.1 and B.2.

After initialization at a feasible point, DOP1 is solved for multiple conversions X_{1C12en} according to Eq. (A.12) by adding the constraint

$$0 = X_{\mathrm{1C12en}} - X_{\mathrm{target}} \tag{B.1}$$

and varying the target conversion X_{target} between 0.2 and 1.0. To ensure feasibility, especially at very high and low conversions, 1 % variation from the target conversion is permitted.

For the experimental validation of the feasibility of the process, the specifications of the available experimental equipment limit the process performance. Therefore, these limitations, especially with respect to the size of the reaction and buffer vessels as well as their stability, need to be taken into account. DOP2 is derived from DOP1 incorporating these limitations but keeping the overall configuration including the CSTR and the apolar recycle from the distillation column. By reducing the degrees of freedom, an operation point denoted as *SS OP w/ CSTR & DistCol* is specified for comparison to the dynamic process model. The resulting optimization problem can be summarized as

$$\min_{u(t)} \quad -S_{\mathrm{nC13al}} \tag{DOP2}$$

s.t.

reaction rates	Eq. $(A.1 - A.11)$,
gas solubility	Eq. $(2 - 3)$,
constitutive equations	Eq. $(A.18 - A.20)$,
component mass balances	Eq. $(A.15 - A.17)$,
	Eq. $(A.21 - A.23, 20)$,
	Eq. $(A.29 - A.30)$,
	Eq. $(A.33 - A.41)$,
phase separation	Eq. $(A.31 - A.32)$,
flowsheet	Eq. $(4 - 9)$,
residence time	Eq. (1),
reactor indices	Eq. $(A.12 - A.14)$,
	$n/iso \geq 0.95$,
initial conditions, LB, UB	Table $B.1$ and $B.3$,
gas phase composition	$\sum_{\alpha \in \mathrm{GAS}} y_\alpha^{\mathrm{SBR}}(t) = 1, \sum_{\alpha \in \mathrm{GAS}} y_\alpha^{\mathrm{CSTR}} = 1,$
	$0 = y_\alpha^{\mathrm{DBuffer}}(t) - y_\alpha^{\mathrm{SBR}}(t_{\mathrm{B}}) \quad \forall \alpha \in \mathrm{GAS},$
stream constraints	$\dot{N}_\alpha(t) \geq 0 \quad \forall \alpha \in \mathrm{SPC} \cup \mathrm{GAS},$
composition constraints	$c_\alpha(t) \geq 0,\, n_\alpha(t) \geq 0 \quad \forall \alpha \in \mathrm{SPC} \cup \mathrm{GAS},$
controls	$u(t) = \left[j_{\mathrm{CO}}^{\mathrm{SBR}}(t), j_{\mathrm{H_2}}^{\mathrm{SBR}}(t) \right].$

Due to smaller vessel sizes, the problem is initialized using

$$m_{\mathrm{1C12en,init}}^{\mathrm{SBR}} = 18\,\mathrm{g}, \qquad \dot{N}_{\mathrm{make-up,init}} = \vec{0}, \qquad n_{\mathrm{init}}^{\mathrm{SBR,gas}} = \frac{y_{\mathrm{init}} p_{\mathrm{init}} V^{\mathrm{gas}}}{\tilde{R}T},$$

as well as Table B.1 and B.3.

For proving the feasibility of a quasi-continuous process operation, the miniplant is constructed without a CSTR or a distillation column. As a consequence, the process model needs to be adapted as well, leading to

$$\min_{u(t),q} \quad -S_{\mathrm{nC13al}} \tag{DOP3}$$

s.t.

reaction rates	Eq. $(A.1 - A.11)$,
gas solubility	Eq. $(2 - 3)$,
constitutive equations	Eq. $(A.18 - A.20)$,
component mass balances	Eq. $(A.15 - A.17)$,
	Eq. $(A.21 - A.23, 20)$,
phase separation	Eq. (A.31 – A.32),
flowsheet	Eq. $(4 - 9)$,
residence time	Eq. (1),
reactor indices	Eq. $(A.12 - A.14)$,
	$n/iso \geq 0.95$,
initial conditions, LB, UB	Table $B.1$ and $B.3$,
gas phase composition	$\sum_{\alpha \in \mathrm{GAS}} y_\alpha^{\mathrm{SBR}}(t) = 1,$
	$0 = y_\alpha^{\mathrm{DBuffer}}(t) - y_\alpha^{\mathrm{SBR}}(t_\mathrm{B}) \quad \forall \alpha \in \mathrm{GAS},$
	Eq. (21),
stream constraints	$\dot{N}_\alpha(t) \geq 0 \quad \forall \alpha \in \mathrm{SPC} \cup \mathrm{GAS},$
composition constraints	$c_\alpha(t) \geq 0,\ n_\alpha(t) \geq 0 \quad \forall \alpha \in \mathrm{SPC} \cup \mathrm{GAS},$
controls	$u(t) = \left[j_{\mathrm{CO}}^{\mathrm{SBR}}(t), j_{\mathrm{H_2}}^{\mathrm{SBR}}(t) \right].$

Calculations using this optimization problem are denoted as *SS OP w/o CSTR & DistCol.*

B.2. Dynamic

For the dynamic process model, the problem formulation leads to two optimization problems which are solved in sequence for each process cycle. The *Idle* stage can be expressed as an optimization problem

$$\begin{aligned} &\min && 0 \\ &\text{s.t.} \\ &\text{reaction rates} && \text{Eq. } (A.1 - A.11), \\ &\text{gas solubility} && \text{Eq. } (2 - 3), \\ &\text{constitutive equations} && \text{Eq. } (A.18 - A.20), \\ &\text{component mass balances} && \text{Eq. } (A.15 - A.17), \\ &\text{initial conditions} && \text{Table } B.4, \\ &\text{composition constraints} && n_\alpha(t) \geq 0 \quad \forall \alpha \in \text{SPC} \cup \text{GAS}, \end{aligned} \tag{DOP4}$$

with the objective function set to zero because of no control variables being available. Here, the gas phase composition y^{SBR} is kept constant at its initial value specified in Table B.4. The initial composition is dependent on the final composition and liquid hold-up of the feed buffer tank of the previous process cycle.

For the subsequent DOP which combines the *Reaction* and *Continuous* stage, two different cases need to be differentiated based on the process configuration of the continuous part. Both cases utilize the SBR model for which optimal control of the temperature, pressure and dosing of gaseous components is generally permitted. When employing the CSTR and the distillation column in addition to the buffer tanks and the decanter, the optimization problem can be expressed with

$$\min_{u(t),\dot{V}_{\text{out}}} \quad -S_{\text{nC13al}} + \left(V_{\text{L}}(t_{\text{D}}) - V_{\text{L,min}}\right)^2_{\text{DBuffer}} \tag{DOP5}$$

s.t.

reaction rates	Eq. $(A.1 - A.11)$,
gas solubility	Eq. $(2 - 3)$,
constitutive equations	Eq. $(A.18 - A.20, A.28)$,
component mass balances	Eq. $(A.15 - A.17)$,
	Eq. $(A.25 - A.27)$,
	Eq. $(A.29 - A.30)$,
	Eq. $(A.33 - A.41)$,
	Eq. $(A.42 - A.44)$,
phase separation	Eq. $(A.31 - A.32)$,
flowsheet	Eq. $(13 - 14)$,
	Eq. $(16 - 19)$,
residence time	Eq. (1),
reactor indices	Eq. $(A.12 - A.14)$,
initial conditions, LB, UB	Table $B.1$ and $B.4$,
gas phase composition	$\sum_{\alpha \in \text{GAS}} y_\alpha^{\text{SBR}}(t) = 1,$
	Eq. (15),
stream constraints	$\dot{N}_\alpha(t) \geq 0 \quad \forall \alpha \in \text{SPC} \cup \text{GAS},$
composition constraints	$n_\alpha(t) \geq 0, c_\alpha(t) \geq 0 \quad \forall \alpha \in \text{SPC} \cup \text{GAS},$
controls	$u(t) = \left[j_{\text{CO}}^{\text{SBR}}(t), j_{\text{H}_2}^{\text{SBR}}(t)\right].$

The selectivity is calculated using Eq. (A.13) and emptying of the flash buffer tank is enforced using a residual liquid hold-up as set-point for the terminal liquid hold-up of the flash buffer tank

in the objective function. This formulation is beneficial in comparison to a formulation using an equality constraint because it allows for convergence to a feasible solution even though emptying of the flash buffer tank might not be possible, i.e. if the terminal constraints on the composition in the feed buffer tank are violated. As initial conditions for the first process cycle,

$$m^{\mathrm{SBR}}_{\mathrm{1C12en,init}} = 18\,\mathrm{g}, \qquad \dot{N}_{\mathrm{make-up,init}} = \vec{0}, \qquad n^{\mathrm{SBR,gas}}_{\mathrm{init}} = \frac{y_{\mathrm{init}} p_{\mathrm{init}} V^{\mathrm{gas}}}{\bar{R}T},$$

are chosen analogous to the case studies of the steady-state model. For subsequent process cycles, the initial conditions are dependent on the *Idle* stage and the amount of fresh substrate which is calculated in the previous process cycle in accordance with Eq. (16-19). To allow for the comparison to the operating point determined for the case *SS OP w/ CSTR & DistCol*, the control variables of the CSTR are fixed.

Similar to DOP5, the optimization problem for the combined *Reaction* and *Continuous* stage without the CSTR and distillation column reads

$$\min_{u(t),\dot{V}_{\text{out}}} \quad -S_{\text{nC13al}} + \left(V_{\text{L}}(t_{\text{D}}) - V_{\text{L,min}}\right)^2_{\text{DBuffer}} \tag{DOP6}$$

s.t.

reaction rates	Eq. $(A.1 - A.11)$,
gas solubility	Eq. $(2 - 3)$,
constitutive equations	Eq. $(A.18 - A.20, A.28)$,
component mass balances	Eq. $(A.15 - A.17)$,
	Eq. $(A.25 - A.27)$,
	Eq. $(A.42 - A.44)$,
phase separation	Eq. $(\text{A}.31 - A.32)$,
flowsheet	Eq. $(13 - 14)$,
	Eq. $(16 - 19)$,
residence time	Eq. (1),
reactor indices	Eq. $(A.12 - A.14)$,
initial conditions	Table $B.1$ and $B.4$,
gas phase composition	$\sum_{\alpha \in \text{GAS}} y_\alpha^{\text{SBR}}(t) = 1,$
	Eq. (15),
	Eq. (21),
stream constraints	$\dot{N}_\alpha(t) \geq 0 \quad \forall \alpha \in \text{SPC} \cup \text{GAS},$
composition constraints	$n_\alpha(t) \geq 0 \quad \forall \alpha \in \text{SPC} \cup \text{GAS},$
controls	$u(t) = \left[j_{\text{CO}}^{\text{SBR}}(t), j_{\text{H}_2}^{\text{SBR}}(t)\right].$

Table B.1: Operating conditions for the decanter and distillation column unit model as well as additional process parameters. The data is taken from Dreimann et al. [5] and Kaiser et al. [1].

	Parameter	[.]	Value
Dec	T	°C	5
DistCol	T_{Dist}	°C	58
	T_{Bott}	°C	138
	$\zeta_{\mathrm{LK}}^{\mathrm{Dist}}$	$\mathrm{mol\,mol^{-1}}$	0.99
	$\zeta_{\mathrm{HK}}^{\mathrm{Dist}}$	$\mathrm{mol\,mol^{-1}}$	0.01
Dec	T	°C	5
Process	$\phi_{\mathrm{C10an,DMF}}$	$\mathrm{g\,g^{-1}}$	1
	$\phi_{\mathrm{C10an,1C12en}}$	$\mathrm{g\,g^{-1}}$	$^{42}/_{16}$
	$\phi_{\mathrm{cat,1C12en}}$	$\mathrm{mol\,mol^{-1}}$	$^{1}/_{4000}$

Table B.2: Process conditions for the reference case using the steady-state model. The data is taken from Hentschel et al. [20] and Kaiser et al. [1].

			SS Reference		
	Parameter	[.]	Init	LB	UB
SBR	T	°C	105	40	115
	$k_\mathrm{L}a(\mathrm{H_2})$	min^{-1}	9.57	-	-
	$k_\mathrm{L}a(\mathrm{CO})$	min^{-1}	7.08	-	-
	V	mL	550	-	-
	ε_L	$\mathrm{mL\,mL}^{-1}$	0.66	-	-
	t_B	min	105	0	∞
	t_I	min	0	-	-
	p_init	bar	21	10	21
	$y_{\mathrm{H_2}}$	–	0.5	0	1
	y_CO	–	0.5	0	1
	$j_{\mathrm{H_2}}$	$\mathrm{mol\,s}^{-1}$	$n^{\mathrm{SBR,gas}}_{\mathrm{H_2,init}}/t_\mathrm{B}$	0	∞
	j_CO	$\mathrm{mol\,s}^{-1}$	$n^{\mathrm{SBR,gas}}_{\mathrm{CO,init}}/t_\mathrm{B}$	0	∞
DBuffer	T	°C	$T^{\mathrm{SBR}}(t_\mathrm{B})$		
	p	bar	$p^{\mathrm{SBR}}(t_\mathrm{B})$		
	$y_{\mathrm{H_2}}$	–	$y^{\mathrm{SBR}}_{\mathrm{H_2}}(t_\mathrm{B})$		
	y_CO	–	$y^{\mathrm{SBR}}_{\mathrm{CO}}(t_\mathrm{B})$		
	$k_\mathrm{L}a(\mathrm{H_2})$	min^{-1}	9.57	-	-
	$k_\mathrm{L}a(\mathrm{CO})$	min^{-1}	7.08	-	-
	$\dot{V}_\mathrm{out}$	$\mathrm{mL\,h}^{-1}$	Eq. (A.24)		
CSTR	T	°C	115	60	115
	p	bar	21	10	21
	$y_{\mathrm{H_2}}$	–	0.5	0	1
	y_CO	–	0.5	0	1
	$k_\mathrm{L}a(\mathrm{H_2})$	min^{-1}	9.57	-	-
	$k_\mathrm{L}a(\mathrm{CO})$	min^{-1}	7.08	-	-
	V	mL	1000	-	-
	ε_L	$\mathrm{mL\,mL}^{-1}$	0.3	-	-
Process	ξ^{Dec}	$\mathrm{mol\,mol}^{-1}$	0	0	1
	ξ^{DistCol}	$\mathrm{mol\,mol}^{-1}$	0	0	1
	n/iso	$\mathrm{mol\,mol}^{-1}$	0.95	0.95	1

Table B.3: Process conditions for the steady-state model w/ and w/o CSTR and distillation column. The data is taken from Hentschel et al. [20], Kaiser et al. [1] and from the experimental setup.

			SS OP w/ CSTR & DistCol			SS OP w/o CSTR & DistCol		
	Parameter	[.]	Init	LB	UB	Init	LB	UB
SBR	T	°C	105	-	-	105	-	-
	$k_\mathrm{L}a(\mathrm{H_2})$	min^{-1}	9.57	-	-	9.57	-	-
	$k_\mathrm{L}a(\mathrm{CO})$	min^{-1}	7.08	-	-	7.08	-	-
	V^*	mL	240	-	-	240	-	-
	ε_L	$\mathrm{mL\,mL}^{-1}$	0.66	-	-	0.66	-	-
	t_B^*	min	60	-	-	60	-	-
	t_I^*	min	30	-	-	30	-	-
	p^*	bar	19	-	-	19	-	-
	$y_{\mathrm{H_2}}$	–	0.5	0	1	0.5	0	1
	y_CO	–	0.5	0	1	0.5	0	1
	$j_{\mathrm{H_2}}$	$\mathrm{mol\,s}^{-1}$	$n_{\mathrm{H_2,init}}^{\mathrm{SBR,gas}}/t_\mathrm{B}$	0	∞	$n_{\mathrm{H_2,init}}^{\mathrm{SBR,gas}}/t_\mathrm{B}$	0	∞
	j_CO	$\mathrm{mol\,s}^{-1}$	$n_{\mathrm{CO,init}}^{\mathrm{SBR,gas}}/t_\mathrm{B}$	0	∞	$n_{\mathrm{CO,init}}^{\mathrm{SBR,gas}}/t_\mathrm{B}$	0	∞
DBuffer	T^*	°C	91	-	-	91	-	-
	p^*	bar	16.21	-	-	16.21	-	-
	$y_{\mathrm{H_2}}$	–	$y_{\mathrm{H_2}}^{\mathrm{SBR}}(t_\mathrm{B})$			$y_{\mathrm{H_2}}^{\mathrm{SBR}}(t_\mathrm{B})$		
	y_CO	–	$y_\mathrm{CO}^{\mathrm{SBR}}(t_\mathrm{B})$			$y_\mathrm{CO}^{\mathrm{SBR}}(t_\mathrm{B})$		
	$k_\mathrm{L}a(\mathrm{H_2})$	min^{-1}	$9.57/10$	-	-	$9.57/10$	-	-
	$k_\mathrm{L}a(\mathrm{CO})$	min^{-1}	$7.08/10$	-	-	$7.08/10$	-	-
	$V_\mathrm{L,min}^*$	mL	25	-	-	25	-	-
	$\dot{V}_\mathrm{out}$	$\mathrm{mL\,h}^{-1}$	Eq. (20)			Eq. (20)		
CSTR	T	°C	115	-	-			
	p	bar	21	-	-			
	$y_{\mathrm{H_2}}$	–	0.5	-	-			
	y_CO	–	0.5	-	-		/	
	$k_\mathrm{L}a(\mathrm{H_2})$	min^{-1}	9.57	-	-			
	$k_\mathrm{L}a(\mathrm{CO})$	min^{-1}	7.08	-	-			
	V	mL	1000	-	-			
	ε_L	$\mathrm{mL\,mL}^{-1}$	0.3	-	-			
Process	ξ^{Dec}	$\mathrm{mol\,mol}^{-1}$	0	-	-	0	-	-
	ξ^{DistCol}	$\mathrm{mol\,mol}^{-1}$	0	-	-		/	
	n/iso	$\mathrm{mol\,mol}^{-1}$	0.95	0	1	0.95	0	1

* Data taken from the experimental setup.

Table B.4: Process conditions for the dynamic model w/ and w/o CSTR and distillation column. The data is taken from Hentschel et al. [20], Kaiser et al. [1] and from the experimental setup.

			Dyn OP w/ CSTR & DistCol			Dyn OP w/o CSTR & DistCol		
	Parameter	[.]	Init	LB	UB	Init	LB	UB
SBR	T	°C	105	-	-	105	-	-
	$k_\mathrm{L}a(\mathrm{H_2})$	min^{-1}	9.57	-	-	9.57	-	-
	$k_\mathrm{L}a(\mathrm{CO})$	min^{-1}	7.08	-	-	7.08	-	-
	V^*	mL	240	-	-	240	-	-
	ε_L	$\mathrm{mL\,mL}^{-1}$	0.66	-	-	0.66	-	-
	t_B^*	min	60	-	-	60	-	-
	t_I^*	min	30	-	-	30	-	-
	p^*	bar	19	-	-	19	-	-
	$y_{\mathrm{H_2}}$	–	0.5	0	1	0.5	0	1
	y_CO	–	0.5	0	1	0.5	0	1
	$j_{\mathrm{H_2}}$	$\mathrm{mol\,s}^{-1}$	$n_{\mathrm{H_2,init}}^{\mathrm{SBR,gas}}/t_\mathrm{B}$	0	∞	$n_{\mathrm{H_2,init}}^{\mathrm{SBR,gas}}/t_\mathrm{B}$	0	∞
	j_CO	$\mathrm{mol\,s}^{-1}$	$n_{\mathrm{CO,init}}^{\mathrm{SBR,gas}}/t_\mathrm{B}$	0	∞	$n_{\mathrm{CO,init}}^{\mathrm{SBR,gas}}/t_\mathrm{B}$	0	∞
DBuffer	T^*	°C	91	-	-	91	-	-
	p_0^*	bar	16.21	-	-	16.21	-	-
	p^*	bar	16.21	0	∞	16.21	0	∞
	$y_{\mathrm{H_2}}$	–	$y_{\mathrm{H_2}}^{\mathrm{SBR}}(t_\mathrm{B})$			$y_{\mathrm{H_2}}^{\mathrm{SBR}}(t_\mathrm{B})$		
	y_CO	–	$y_\mathrm{CO}^{\mathrm{SBR}}(t_\mathrm{B})$			$y_\mathrm{CO}^{\mathrm{SBR}}(t_\mathrm{B})$		
	$k_\mathrm{L}a(\mathrm{H_2})$	min^{-1}	$^{9.57}/_{10}$	-	-	$^{9.57}/_{10}$	-	-
	$k_\mathrm{L}a(\mathrm{CO})$	min^{-1}	$^{7.08}/_{10}$	-	-	$^{7.08}/_{10}$	-	-
	V^*	mL	430	-	-	430	-	-
	$V_\mathrm{L,min}^*$	mL	25	-	-	25	-	-
	$\dot{V}_\mathrm{out}$	$\mathrm{mL\,h}^{-1}$	$V_\mathrm{L}^{\mathrm{SBR}}(t_\mathrm{B})/t_\mathrm{D}$	0	∞	$V_\mathrm{L}^{\mathrm{SBR}}(t_\mathrm{B})/t_\mathrm{D}$	0	∞
CSTR	T	°C	115	-	-			
	p	bar	21	-	-			
	$y_{\mathrm{H_2}}$	–	0.5	-	-			
	y_CO	–	0.5	-	-		/	
	$k_\mathrm{L}a(\mathrm{H_2})$	min^{-1}	9.57	-	-			
	$k_\mathrm{L}a(\mathrm{CO})$	min^{-1}	7.08	-	-			
	V	mL	1000	-	-			
	ε_L	$\mathrm{mL\,mL}^{-1}$	0.3	-	-			
UBuffer	T^*	°C	96	-	-	96	-	-
	p_0^*	bar	2.875	-	-	2.875	-	-
	p^*	bar	2.875	0	∞	2.875	0	∞
	$y_{\mathrm{H_2}}$	–	0.5	-	-	0.5	-	-
	y_CO	–	0.5	-	-	0.5	-	-
	$k_\mathrm{L}a(\mathrm{H_2})$	min^{-1}	$^{9.57}/_{10}$	-	-	$^{9.57}/_{10}$	-	-
	$k_\mathrm{L}a(\mathrm{CO})$	min^{-1}	$^{7.08}/_{10}$	-	-	$^{7.08}/_{10}$	-	-
	V^*	mL	260	-	-	260	-	-
Process	ξ^{Dec}	$\mathrm{mol\,mol}^{-1}$	0	-	-	0	-	-
	ξ^{DistCol}	$\mathrm{mol\,mol}^{-1}$	0	-	-		/	
	n/iso	$\mathrm{mol\,mol}^{-1}$	0.95	0.95	1	0.95	0	1

* Data taken from the experimental setup.

C. Steady-State Model Validation

To ensure plausible results of the steady-state model, it is tested in an optimization study in which DOP1 is solved for a sequence of different conversion levels X_{target} between 0.2 and 1.0. Multiple studies are performed with increasing and decreasing conversion targets to prevent running into local optima. Instead of specifying variable liquid hold-ups in the CSTR which allows for a reduced residence time and, as a consequence, reduced conversion (compare [1]), the lower bound of the SBR as well as the CSTR are set to 40 °C and 60 °C, respectively, enabling a reduction in the reaction activity in the corresponding process unit. Except for this change in the formulation of the optimization problem, the process conditions are kept as close as possible to those used in Kaiser et al. [1] (see Table B.1 and B.2), i. e. by setting the temperature and pressure of the flash buffer tank equal to the values of the SBR, keeping the $k_{\text{L}}a$ values constant even though no stirring is present in the buffer tank and by assuming the SBR preparation time to be $t_{\text{I}} = 0\,\text{s}$.

Figure 8 contains the results of the optimization study, represented by the selectivity - conversion behavior of the process setup. Additionally, the operating point (OP) of the detailed design by Kaiser et al. [1] at a selectivity of $S_{\text{nC13al}}^{\text{opt,Kaiser}} = 94.9\,\%$ and conversion $X_{\text{1C12en}}^{\text{opt,Kaiser}} = 98.3\,\%$ is shown for comparison.

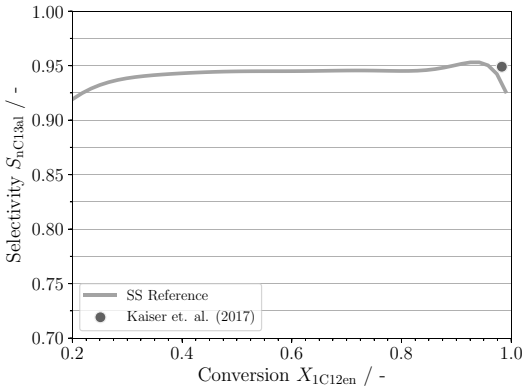

Figure 8: Comparison of the steady-state model using the *SS Reference* case (DOP1) and the model proposed by Kaiser et al. [1].

With a minor difference of $\Delta S_{\text{nC13al}}^{\text{opt}} = 1.1\,\%$ at the same conversion, both steady-state models

generate similar results. It needs to be mentioned that the maximum performance predicted by Kaiser et al. [1], especially for low conversions, lies below the predictions of the present study. One possible explanation for the mismatch is the occurrence of multiple local optima which have been observed for this process setup.

D. Model Comparison

In the following, the concentration profiles in the SBR are shown in cyclic steady-state. The results from the steady-state model are compared to the cyclic steady-state of the dynamic process model for the full process configuration.

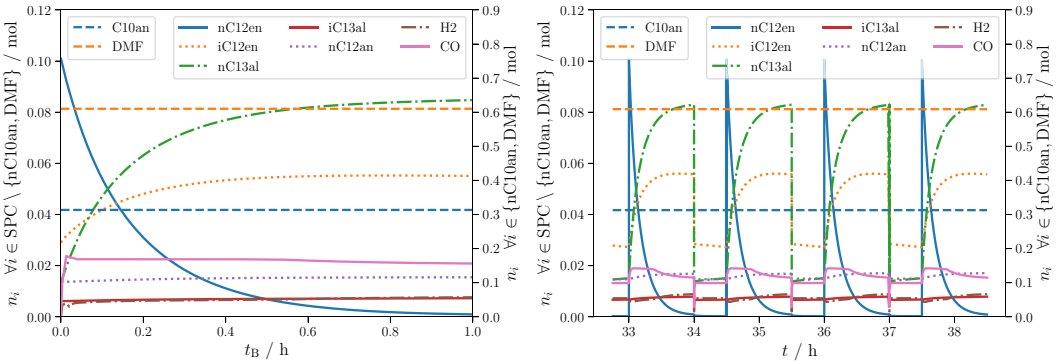

(a) Steady-state model.

(b) Batch cycle 22 to 25 of the dynamic model.

Figure 9: SBR concentration profiles for the full process configuration.

Highlights:

- Manual for modeling a cyclic semi-batch reactor in a continuous process
- Simulations indicate a prolonged start-up time for the hydroformylation process
- Experimental prove of concept of a cyclic hydroformylation process in a TMS-system